Hepatic HAX-1 inactivation prevents metabolic diseases by enhancing mitochondrial activity and bile salt export

Received for publication, December 17, 2019, and in revised form, February 4, 2020 Published, Papers in Press, February 20, 2020, DOI 10.1074/jbc.RA119.012361

Fawzi Alogaili[‡§], Sivaprakasam Chinnarasu[‡], Anja Jaeschke[‡], Evangelia G. Kranias[§], and David Y. Hui[‡1]

From the [‡]Department of Pathology and Laboratory Medicine, Metabolic Diseases Research Center, University of Cincinnati College of Medicine, Cincinnati, Ohio 45237 and the [§]Department of Pharmacology and Systems Physiology, University of Cincinnati College of Medicine, Cincinnati, Ohio 45267

Edited by Jeffrey E. Pessin

Increasing hepatic mitochondrial activity through pyruvate dehydrogenase and elevating enterohepatic bile acid recirculation are promising new approaches for metabolic disease therapy, but neither approach alone can completely ameliorate disease phenotype in high-fat diet–fed mice. This study showed that diet-induced hepatosteatosis, hyperlipidemia, and insulin resistance can be completely prevented in mice with liver-specific HCLS1-associated protein X-1 (HAX-1) inactivation. Mechanistically, we showed that HAX-1 interacts with inositol 1,4,5-trisphosphate receptor-1 (InsP3R1) in the liver, and its absence reduces InsP3R1 levels, thereby improving endoplasmic reticulum–mitochondria calcium homeostasis to prevent excess calcium overload and mitochondrial dysfunction. As a result, HAX-1 ablation activates pyruvate dehydrogenase and increases mitochondria utilization of glucose and fatty acids to prevent hepatosteatosis, hyperlipidemia, and insulin resistance. In contrast to the reduction of InsP3R1 levels, hepatic HAX-1 deficiency increases bile salt exporter protein levels, thereby promoting enterohepatic bile acid recirculation, leading to activation of bile acid–responsive genes in the intestinal ileum to augment insulin sensitivity and of cholesterol transport genes in the liver to suppress hyperlipidemia. The dual mechanisms of increased mitochondrial respiration and enterohepatic bile acid recirculation due to improvement of endoplasmic reticulum–mitochondria calcium homeostasis with hepatic HAX-1 inactivation suggest that this may be a potential therapeutic target for metabolic disease intervention.

The prevalence of metabolic diseases, including obesity, diabetes, and nonalcoholic fatty liver disease, is approaching pandemic proportions worldwide (1–3). These numbers continue to escalate, and traditional strategies currently used for diabetes and nonalcoholic fatty liver disease management have limited success with efficacy, safety, and tolerability issues (4–8). The most successful approach for metabolic disease intervention is bariatric surgery (9). The metabolic improvement of bariatric surgery has been attributed to numerous mechanisms, including altering nutrient transport to bypass the proximal intestine with rapid delivery to the distal intestine, changes in the gut microbiota, and increasing bile salt transport in the enterohepatic circulation (10–14). The metabolic benefits of enhanced bile salt circulation are due to the activation of the membrane receptor Takeda-G-protein receptor-5 to increase energy expenditure in adipose tissues, the promotion of glucagon-like peptide-1 release by L-cells to stimulate β cell insulin secretion (15), and the activation of fibroblast growth factor-19 (FGF19;[2] FGF15 in mice) synthesis in the distal intestinal ileum to improve glucose metabolism in hepatic and extrahepatic tissues (16, 17).

Emerging evidence indicates that mitochondrial dysfunction may be a key driver for metabolic disease manifestation (18), and improving calcium homeostasis through cross-talks between ER and mitochondria in the liver has been suggested as a less invasive approach to maintain glucose and lipid homeostasis for metabolic disease intervention (19, 20). The importance of exquisitely regulated hepatic calcium homeostasis in metabolic disease modulation is highlighted by studies showing that increased ER calcium uptake through overexpression of the sarco(endo)plasmic reticulum Ca^{2+} ATPase-2 (SERCA2) in the liver or reducing ER calcium release through suppression of InsP3R1 not only alleviates ER stress but also improves glucose tolerance, lowers blood glucose levels, and reduces liver steatosis (21–23).

A target with the potential to reap the dual benefits of enhanced enterohepatic bile salt circulation and improved calcium homeostasis and mitochondrial respiration is the hema-

This work was supported by National Institutes of Health Grant RO1 DK074932 (to D. Y. H.). This work was also supported by a scholarship from the Higher Committee for Education Development in Iraq (to F. A.). The authors declare that they have no conflicts of interest with the contents of this article. The content is solely the responsibility of the authors and does not necessarily represent the official views of the National Institutes of Health.

This article contains Tables S1 and S2.

[1] To whom correspondence should be addressed: Dept. of Pathology, University of Cincinnati College of Medicine, 2120 E. Galbraith Rd., Cincinnati, OH 45237. Tel.: 513-558-9152; Fax: 513-558-1312; E-mail: huidy@ucmail.uc.edu.

[2] The abbreviations used are: FGF, fibroblast growth factor; HAX-1, HCLS1-associated protein X-1; InsP3R1, inositol 1,4,5-trisphosphate receptor-1; ER, endoplasmic reticulum; SERCA2, sarco(endo)plasmic reticulum Ca^{2+} ATPase-2; BSEP/ABCB11, bile salt exporter protein/ATP-binding cassette subfamily B member 11; AAV, adeno-associated virus; TBG, thyroxin-binding globulin; OCR, oxygen consumption rate; HOMA-IR, homeostatic assessment of insulin resistance; FCCP, carbonyl cyanide *p*-trifluoromethoxyphenylhydrazone; PDH, pyruvate dehydrogenase; PDK, pyruvate dehydrogenase kinase; StAR, steroidogenic acute response protein; SREBP-1, sterol regulatory element–binding protein-1; LDL, low-density lipoprotein; VLDL, very low-density lipoprotein; IDL, intermediate-density lipoprotein; HDL, high-density lipoprotein; NEFA, nonesterified fatty acid; FPLC, fast-performance liquid chromatography; AUC, area under the curve.

topoietic cell-specific protein-associated protein X-1 (HAX-1). Despite its name, HAX-1 is ubiquitously expressed, with the highest levels observed in liver, kidney, testis, and heart (24). This protein is associated with the cytosolic face of the mitochondria and the ER (25), via sequences found in the amino- and carboxyl-terminal domains, respectively (26), where it modulates calcium cycling between these organelles and regulation of mitochondrial potential (27–30). HAX-1 also has tissue-specific functions that depend on the presence or absence of specific HAX-1–interacting partners in each cell type. For example, in the heart, HAX-1 interacts with phospholamban and heat shock protein 90 to regulate Ca^{2+} cycling and prevent ER stress, respectively, to protect against ischemic heart injury (31, 32). In the liver, where phospholamban is not expressed, HAX-1 binds to the bile salt export protein (BSEP), and its absence increases BSEP localization to the bile canaliculus membrane to enhance enterohepatic bile acid recirculation (33).

Whether HAX-1 expression in the liver influences mitochondrial respiration and bile salt homeostasis, and the consequential effects on diet-induced metabolic diseases, have not been explored. This study compares glucose and lipid homeostasis in WT and liver-specific HAX-1 knockout mice after Western diet feeding with the goal of determining whether hepatic HAX-1 is a target for metabolic disease intervention.

Results

HAX-1 is localized at mitochondria and ER in liver, and its inactivation has no deleterious effects in liver

HAX-1 is highly expressed in the liver (24), and its level of expression was similar between chow- and Western diet–fed mice. Its level of expression was also similar regardless of fasting or fed conditions (Fig. 1*A*). Initial characterization of HAX-1 distribution in the liver revealed its predominant location in the mitochondria and the ER (Fig. 1*B*). To explore the physiological functions of HAX-1 in the liver, we injected 5×10^{11} genome copies of recombinant AAV8 virus encoding the *Cre* recombinase gene under the control of the strong liver-specific thyroxin-binding globulin (TBG) promoter into *Hax1*$^{flox/flox}$ mice (30, 34), which effectively eliminated HAX-1 expression specifically in the liver, whereas injection of the control vector expressing the GFP, AAV-TBG-GFP, had no effect on HAX1 expression (Fig. 1*C*). Histological examination as well as plasma alanine aminotransferase measurements revealed no abnormalities, and HAX-1 inactivation does not cause liver injury, fibrosis, or toxicity (Fig. 1, *D* and *E*). Thus, all subsequent experiments comparing the impact of liver-specific Hax-1 inactivation were performed by using *Hax1*$^{flox/flox}$ mice injected with AAV-TBG-GFP as control mice and those injected with AAV-TBG-*Cre* as liver-specific *Hax1* knockout (L-Hax1$^{-/-}$) mice.

Hepatic HAX-1 deficiency reduces plasma triglyceride levels in chow-fed mice

Significantly lower fasting plasma triglyceride and VLDL levels, but not total cholesterol, IDL/LDL, or HDL levels, were observed in chow-fed L-Hax1$^{-/-}$ mice compared with control mice (Fig. 2, *A* and *B*). Fasting plasma nonesterified fatty acid levels were also similar between chow-fed control and L-Hax1$^{-/-}$ mice (Fig. 2*C*). The difference in plasma triglyceride and VLDL levels in control and L-Hax1$^{-/-}$ mice was not due to differences in VLDL synthesis and secretion (Fig. 2*D*). However, when control and L-Hax1$^{-/-}$ mice were administered a bolus lipid meal after an overnight fast, the L-Hax1$^{-/-}$ mice showed a trend toward less postprandial hypertriglyceridemia, indicative of accelerated clearance, although area under the curve analysis revealed that the difference did not reach statistical significance (Fig. 2*E*).

L-Hax1$^{-/-}$ mice sustain euglycemia with lower insulin levels

Fasting blood glucose levels were similar and within normal range in both age-matched control *Hax1*$^{flox/flox}$ mice and L-Hax1$^{-/-}$ mice (Fig. 3*A*). Interestingly, whereas fasting insulin levels in the control mice were similar and within the normal range observed with WT mice, fasting insulin levels were significantly lower in L-Hax1$^{-/-}$ mice compared with the control mice (Fig. 3*B*), leading to a lower homeostatic model assessment-insulin resistance (HOMA-IR) index suggestive of elevated insulin sensitivity in mice with liver HAX-1 inactivation (Fig. 3*C*). Indeed, an oral glucose tolerance test administered after an overnight fast showed decreased glucose excursion in L-Hax1$^{-/-}$ mice (Fig. 3*D*). Taken together, these results indicate that the L-Hax1$^{-/-}$ mice are capable of maintaining euglycemia with lower insulin levels by a mechanism that is consistent with improved glucose tolerance and insulin sensitivity.

Hepatic HAX-1 inactivation protects against Western diet–induced hyperlipidemia, hyperinsulinemia, and hepatosteatosis

The low plasma triglyceride levels and their ability to maintain euglycemia with low basal fasting insulin levels in chow-fed L-Hax1$^{-/-}$ mice prompted us to investigate the influence of liver HAX-1 inactivation on metabolic disease manifestation in response to chronic feeding of a high-fat/cholesterol-type Western diet. The L-Hax1$^{-/-}$ mice displayed a slightly lower body weight and adiposity compared with control mice after 12 weeks of Western diet feeding, but the difference did not reach statistical significance (Fig. 4*A*). The marginal differences in body weight cannot be attributed to differences in food intake. In fact, food intake appeared to be higher in L-Hax1$^{-/-}$ mice compared with control mice (4.3 ± 0.35 g/day *versus* 3.6 ± 0.4 g/day). Both the control and the L-Hax1$^{-/-}$ mice were capable of maintaining euglycemia throughout the 12-week Western diet feeding period, and neither group developed overt hyperglycemia (Fig. 4*B*). However, the control mice developed hyperinsulinemia, indicative of prediabetes and insulin resistance, whereas insulin levels in the L-Hax1$^{-/-}$ mice remained at low or normal levels, indicative of resistance to diet-induced hyperinsulinemia (Fig. 4*B*). Estimation of insulin resistance by HOMA-IR is consistent with the interpretation that the control mice became insulin-resistant after 12 weeks of Western diet feeding, but the L-Hax1$^{-/-}$ mice remained insulin-sensitive (Fig. 4*B*). Glucose tolerance test after oral administration of a glucose solution as well as insulin sensitivity test administered by insulin injection confirmed that the Western diet–fed control mice were glucose-intolerant and insulin-resistant but the L-Hax1$^{-/-}$ mice remained glucose-tolerant and

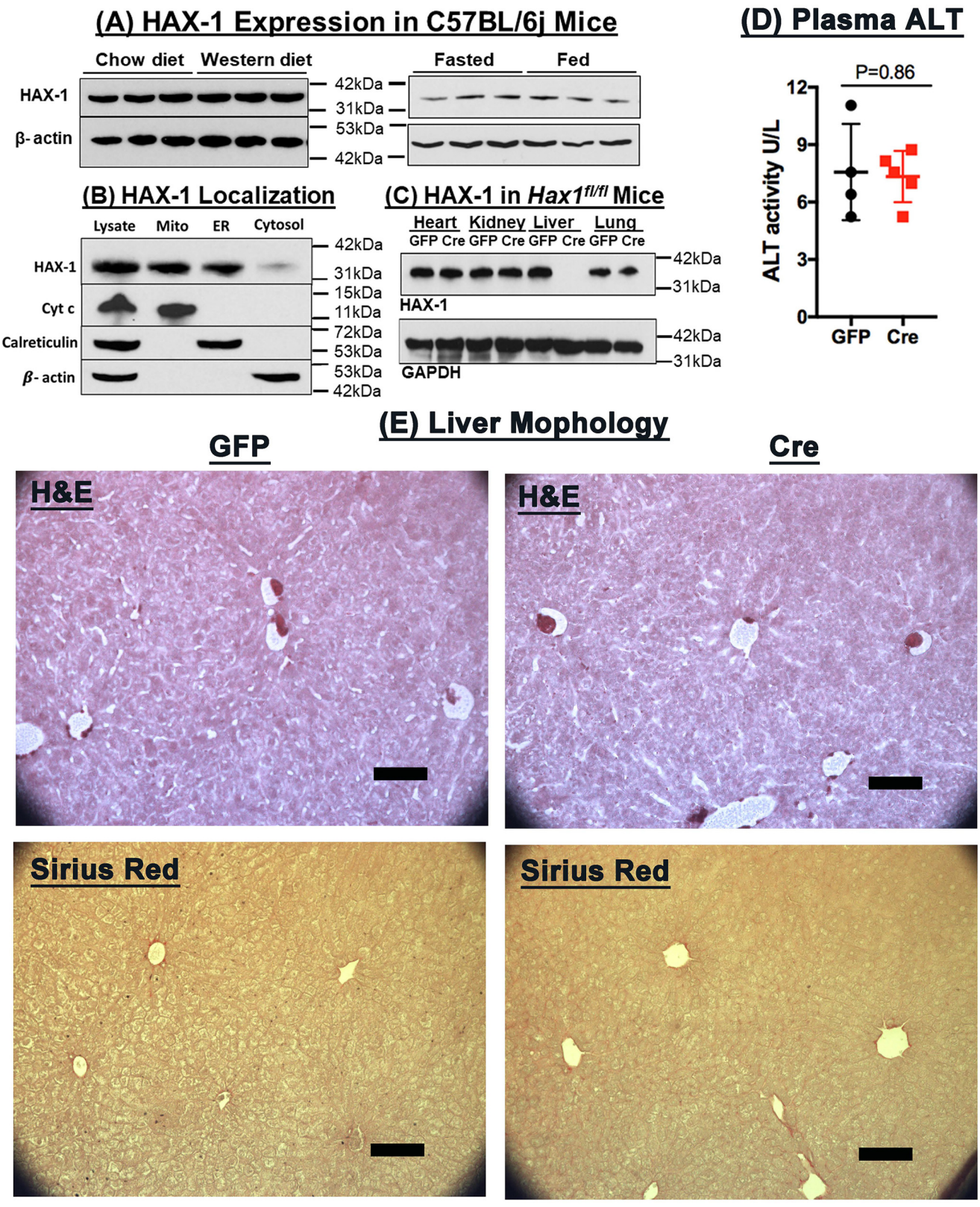

Figure 1. HAX-1 localized to the mitochondria and ER in liver and its absence has no effect on liver morphology. *A*, representative Western blot of $n = 3$ experiments showing HAX-1 protein levels in C57BL/6j mice fed either chow or Western diet, as well as under fasting or fed conditions. *B*, representative Western blot of $n = 3$ experiments showing HAX-1 protein abundance in mitochondria (*Mt*) and ER fractions prepared from liver lysates, using cytochrome *c* (*CytoC*), calreticulin, and β-actin as markers for mitochondria, ER, and cytosol, respectively. *C*, representative Western blot of $n = 3$ experiments showing HAX-1 protein abundance in tissue homogenates of AAV-TBG-GFP–injected control or AAV-TBG-*Cre*–injected L-Hax1$^{-/-}$ mice. *D*, plasma ALT levels in control (GFP, $n = 4$) or L-Hax1$^{-/-}$ (*Cre*, $n = 5$) mice. Statistics were evaluated by Student's *t* test. *E*, histological staining with hematoxylin and eosin (*H&E*) and Sirius Red of sections prepared from livers of chow-fed control (GFP) and L-Hax1$^{-/-}$ (*Cre*) mice ($n = 6$). *Scale bars*, 100 μm. *Error bars*, S.D.

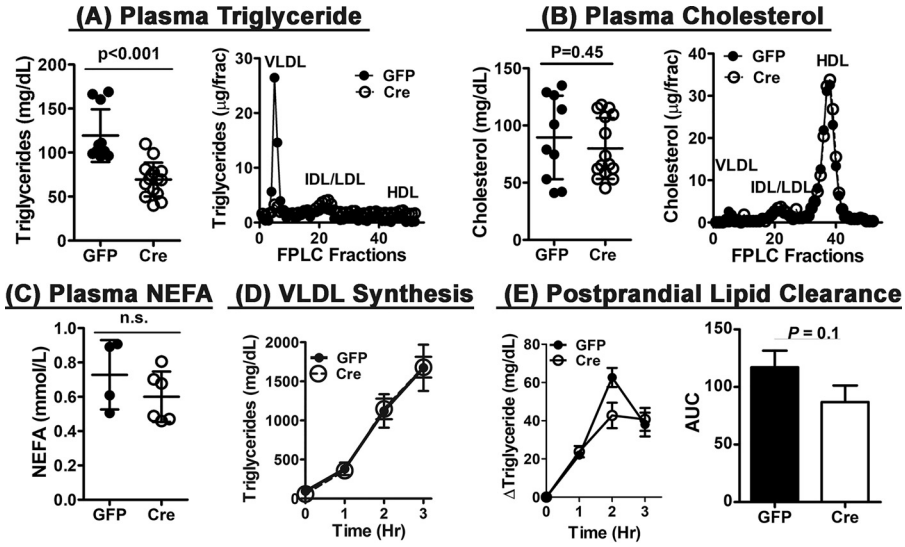

Figure 2. Hepatic HAX-1 deficiency reduces plasma triglyceride levels in chow-fed mice. *Hax1*$^{flox/flox}$ mice were injected with AAV-TBG-GFP or AAV-TBG-*Cre*. *A* and *B*, fasting plasma triglyceride and cholesterol levels and representative lipid distribution among various lipoprotein classes were measured from GFP- and *Cre*-injected mice (10–12 mice/group). *C*, fasting plasma NEFA levels were measured from four GFP- and six *Cre*-injected mice. *D*, VLDL synthesis and secretion from GFP-injected ($n = 7$) and *Cre*-injected ($n = 9$) mice were monitored hourly after Poloxamer 407 injection into fasted mice to inhibit lipolysis. *E*, postprandial lipid clearance was measured based on changes from fasting triglyceride levels in GFP- and *Cre*-injected mice ($n = 6$) after receiving 200 μl of olive oil by oral gavage. All data represent the mean ± S.D. (*error bars*) with the indicated *p* values evaluated by two-tailed Student's *t* test.

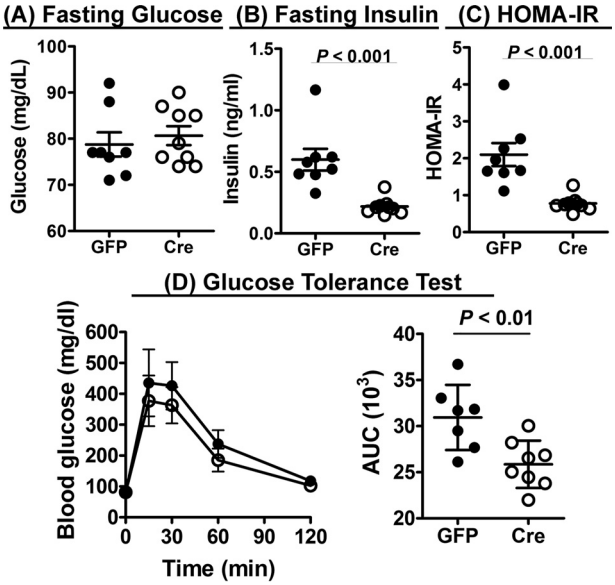

Figure 3. L-Hax1$^{-/-}$ mice sustain euglycemia with lower insulin levels. Shown are fasting blood glucose (*A*) and insulin levels (*B*) in GFP- and *Cre*-injected *Hax1*$^{flox/flox}$ mice after an overnight fast ($n = 8$–9 mice in each group). *C*, the HOMA-IR index was calculated from the raw data. *D*, a bolus glucose solution (2 g/kg body weight) was administered to seven GFP-injected (*solid symbols*) and eight *Cre*-injected (*open symbols*) L-Hax1$^{flox/flox}$ mice after an overnight fast. Blood glucose levels were monitored over a 2-h period to determine glucose tolerance. Area under the curve (AUC) analysis of the data was used for statistical evaluation. All data represent the mean ± S.D. (*error bars*) with the indicated *p* values determined by two-tailed Student's *t* test.

insulin-sensitive 12 weeks after feeding the Western-type diet (Fig. 4, *C* and *D*).

Interestingly, the L-Hax1$^{-/-}$ mice displayed lower fasting plasma nonesterified fatty acid (NEFA) levels compared with control mice under Western diet–feeding conditions (Fig. 4*E*). Importantly, plasma triglyceride and cholesterol levels throughout the 12-week period also remained at normal levels of <100 mg/dl in the L-Hax1$^{-/-}$ mice in contrast to the hyperlipidemia observed in control mice (Fig. 4*F*). Differences in plasma triglyceride and cholesterol levels were reflected by the lower plasma VLDL and LDL levels in L-Hax1$^{-/-}$ mice (Fig. 4*F*). Examination of the livers from Western diet–fed control and L-Hax1$^{-/-}$ mice revealed significant steatosis with more triglyceride and cholesterol in the livers of control mice compared with that observed in L-Hax1$^{-/-}$ mice (Fig. 5). Thus, in addition to protection against diet-induced hyperlipidemia and glucose intolerance, hepatic HAX-1 deficiency also protects against fatty liver disease.

Hepatic HAX-1 deficiency suppresses glucose-induced lipogenesis

To examine the mechanism underlying the differences in plasma lipid levels and hepatosteatosis susceptibility between control and L-Hax1$^{-/-}$ mice, primary hepatocytes isolated from these animals were incubated in media containing 5 and 25 mM glucose to mimic normal and hyperglycemic conditions and then assayed for triglyceride content in cell lysate and in the extracellular medium. In the presence of 5 mM glucose, no difference in intracellular triglyceride content was observed between control and L-Hax1$^{-/-}$ hepatocytes (Fig. 6*A*). However, in the presence of 25 mM glucose, an ~2.5-fold increase in intracellular triglyceride content was observed in control hepatocytes but the L-Hax1$^{-/-}$ hepatocytes did not display glucose-induced steatosis, and their intracellular triglyceride levels remained similar to those observed in control and L-Hax1$^{-/-}$ hepatocytes cultured under normoglycemic conditions (Fig. 6*A*). The L-Hax1$^{-/-}$ hepatocytes also secrete less triglyceride into the medium under normoglycemic conditions (Fig. 6*A*). Whereas hyperglycemic conditions increased the triglyceride levels in the medium of L-Hax1$^{-/-}$ hepatocytes to levels similar to those observed when control hepatocytes were cultured under normoglycemic conditions, significantly more triglycerides were found in the media of the

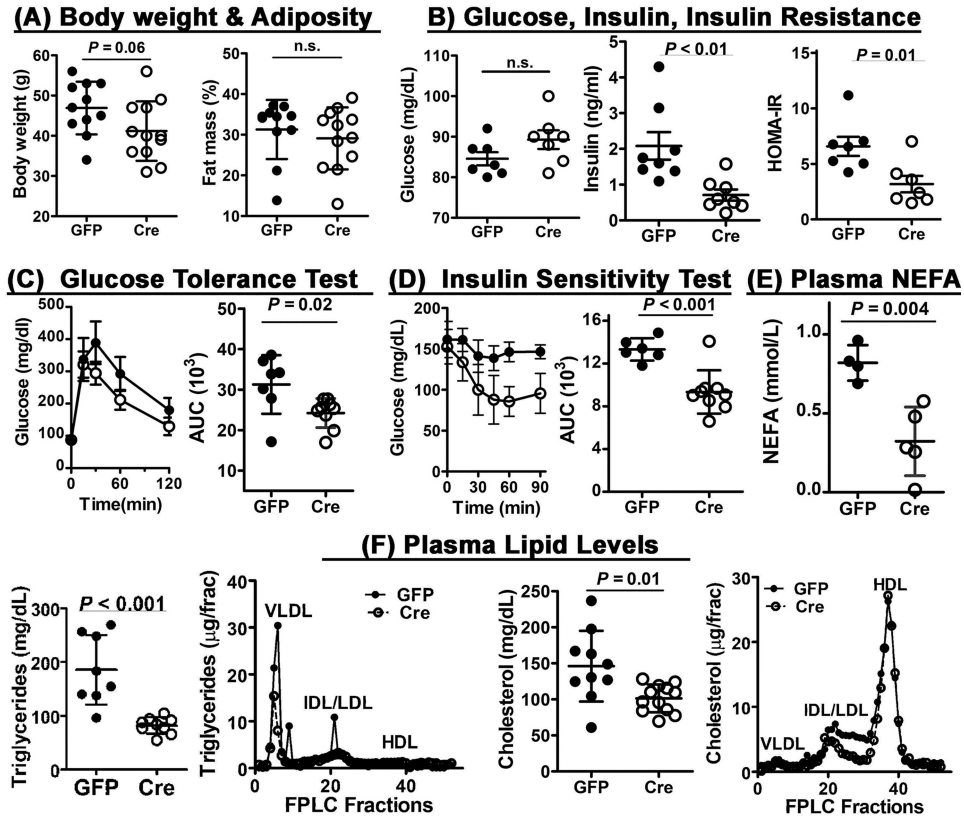

Figure 4. Hepatic HAX-1 inactivation protects against Western diet–induced hyperlipidemia and hyperinsulinemia. *Hax1*$^{flox/flox}$ mice injected with AAV-TBG-GFP or AAV-TBG-*Cre* were fed a Western type diet for 12 weeks. *A*, body weights and adiposity were determined from 11 GFP-injected and 12 *Cre*-injected mice. *B*, fasting blood glucose and insulin levels were measured from eight mice in each group, and the data were used for HOMA-IR estimation of insulin resistance. *C*, blood glucose levels were monitored after the administration of a bolus glucose solution (2 g/kg body weight) to Western diet–fed control (*solid symbols*) and L-Hax1$^{-/-}$ mice (*open symbols*) ($n = 7$). The data were used to calculate AUC for statistical analysis. *D*, blood glucose levels were monitored after insulin injection (0.75 units/kg body weight) into Western diet–fed control (*solid symbols*; $n = 6$) and L-Hax1$^{-/-}$ mice (*open symbols*; $n = 9$), and AUC was calculated based on the data. *E*, fasting plasma NEFA levels were measured from four GFP- and six *Cre*-injected mice. *F*, fasting plasma triglyceride and cholesterol levels were measured from eight mice in each group. Samples were pooled from three mice in each group for FPLC analysis of lipoprotein distribution. All data represent the mean ± S.D. (*error bars*) with the indicated *p* values determined by two-tailed Student's *t* test.

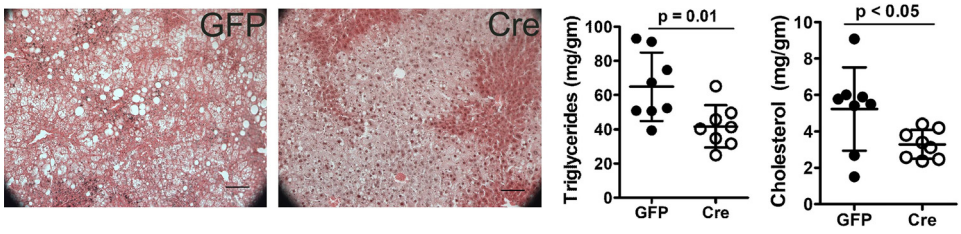

Figure 5. Hepatic HAX-1 inactivation reduces Western diet–induced liver steatosis. *A*, representative images of hematoxylin-eosin–stained liver sections from Western diet–fed control (GFP) and L-Hax1$^{-/-}$ (*Cre*) mice ($n = 8$ in each group). *Scale bars*, 100 µm. Hepatosteatosis was quantified by measuring liver triglyceride and cholesterol levels ($n = 8$ in each group). *Error bars*, S.D.

control hepatocytes when cultured with 25 mM glucose (Fig. 6*A*). These *in vitro* data were corroborated with *in vivo* experiments showing reduced *de novo* lipogenesis in the liver of L-Hax1$^{-/-}$ mice (Fig. 6*B*). Furthermore, although no statistically significant differences were observed in VLDL secretion between control and L-Hax1$^{-/-}$ mice (Fig. 2*E*), postprandial VLDL secretion after a bolus glucose meal was significantly reduced in L-Hax1$^{-/-}$ mice (Fig. 6*C*). Taken together, these results indicate that hepatic HAX-1 inactivation reduces glucose-induced lipogenesis and thereby lowers plasma triglyceride levels and protects against diet-induced hepatosteatosis in L-Hax1$^{-/-}$ mice.

Hepatic HAX-1 deficiency increases mitochondrial respiration and fatty acid oxidation

The reduced glucose-induced lipogenesis with the consequential effects of lower plasma triglyceride levels and suppression of hepatosteatosis observed in L-Hax1$^{-/-}$ mice suggested that hepatic HAX-1 deficiency may increase glucose utilization. To test this possibility, primary hepatocytes isolated from control and L-Hax1$^{-/-}$ mice were incubated with normal medium containing 25 mM glucose, and oxygen consumption rates were monitored over a 2-h period. Oligomycin was added to inhibit ATP synthesis, followed by carbonyl cyanide *p*-trifluoromethoxyphenylhydrazone (FCCP)

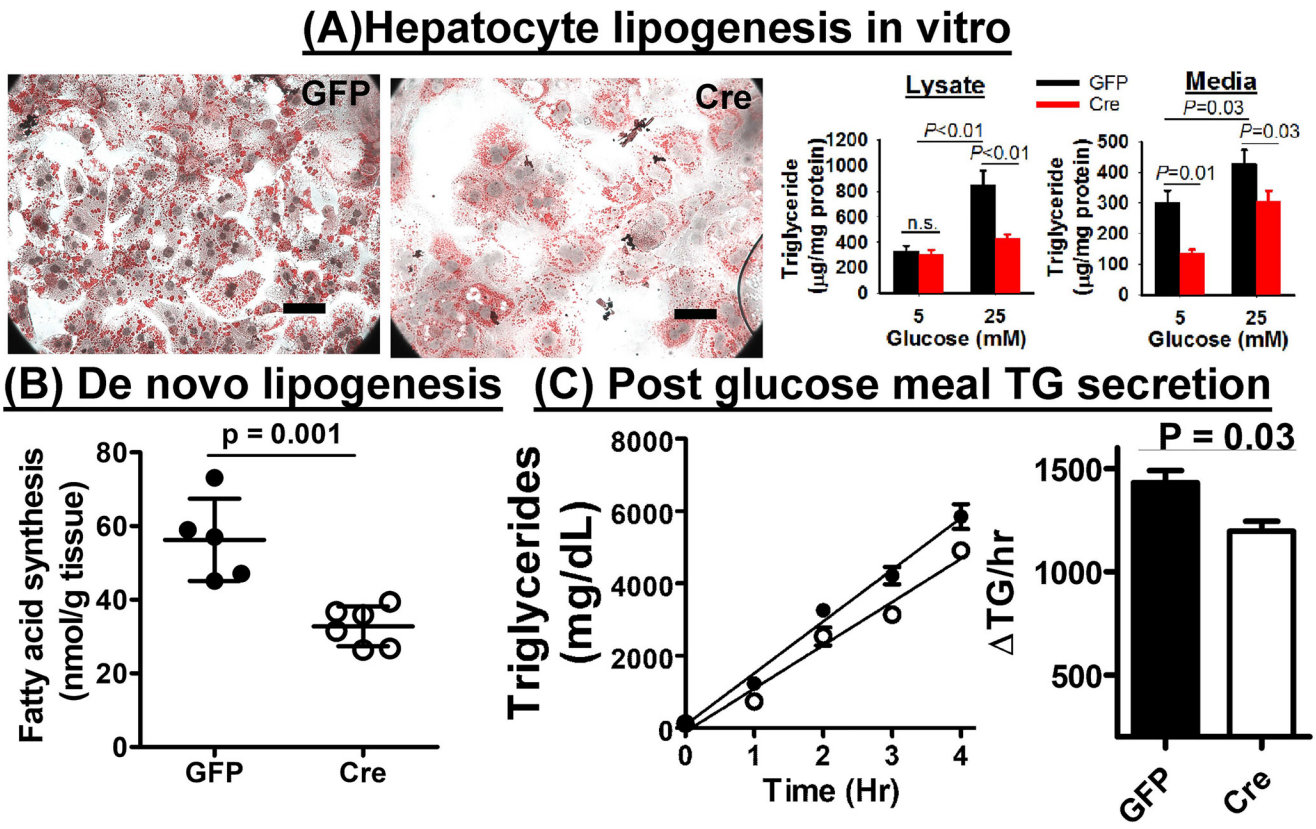

Figure 6. Hepatic HAX-1 inactivation suppresses *de novo* lipogenesis and postprandial VLDL secretion. *A*, primary hepatocytes isolated from control (GFP) and L-Hax1$^{-/-}$ (*Cre*) mice were cultured with 5 or 25 mM glucose. Cell lysates and culture media were collected for triglyceride determinations (n = 4/group). Representative images of Oil Red O–stained hepatocytes after incubation with 25 mM glucose were also shown. *Scale bars*, 100 μm. *B*, *in vivo de novo* lipogenesis was performed by feeding fasted control (GFP) and L-Hax1$^{-/-}$ (*Cre*) mice (n = 6) with 2 mg/g [^{14}C]glucose. The incorporation of the radiolabel into lipids was determined after 2 h. *C*, postprandial VLDL secretion was monitored by Poloxamer 407 injection after acute feeding of a glucose meal to four control (GFP, *filled symbols*) and four L-Hax1$^{-/-}$ (*Cre*, *open symbols*) mice. Differences in VLDL secretion were assessed based on changes in plasma triglyceride levels per hour. All data represent the mean ± S.D. (*error bars*) with the indicated p values determined by Student's t test.

for mitochondria uncoupling and measurement of mitochondrial respiratory capacity, and then rotenone and antimycin A were added to inhibit complex 1 for measurement of nonmitochondrial respiration. Results revealed a significant increase in basal and maximal respiration rates as well as ATP production by hepatocytes from L-Hax1$^{-/-}$ mice compared with hepatocytes isolated from control mice (Fig. 7*A*). However, spare respiration capacity and coupling efficiency were not different between L-Hax1$^{-/-}$ and control hepatocytes (Fig. 7*A*). The latter observations indicated that HAX-1 deficiency improves normal mitochondrial respiration that is unrelated to reserve respiratory capacity in response to stress or energy dissipation as heat.

When oxygen consumption rates were measured in response to 150 μM palmitate in the presence or absence of the fatty acid oxidation inhibitor etomoxir to assess fatty acid–specific oxidation, we found that the L-Hax1$^{-/-}$ hepatocytes also displayed significantly higher oxygen consumption and ATP production in response to fatty acids compared with control hepatocytes (Fig. 7*B*). Moreover, HAX-1–deficient hepatocytes also displayed increased conversion of [^{3}H]palmitate to ^3H_2O (Fig. 7*B*). Consistent with the higher fatty acid oxidation rates of L-Hax1$^{-/-}$ hepatocytes, NEFA levels were found to be lower in the livers of L-Hax1$^{-/-}$ mice (Fig. 7*B*).

The increased mitochondrial oxidation observed in HAX-1–deficient hepatocytes was not due to differences in mitochondria number as indicated by similar ratio of mitochondrially encoded NADH:ubiquinone oxidoreductase (ND1) gene to nuclearly encoded hexokinase-2 (HK2) gene in the livers of control and L-Hax1$^{-/-}$ mice (Fig. 8). Analysis of hepatic RNA expression revealed that HAX-1 inactivation altered the expression of selected fatty acid oxidation genes, particularly under Western diet conditions, including increased expression of carnitine palmitoyltransferase-1 and -2 (*Cpt1* and *Cpt2*), which are responsible for fatty acid transport into the mitochondria, enoyl-CoA hydratase-1 (*Echs1*), which participates in mitochondrial β-oxidation, and cluster of differentiation 36 (*Cd36*), which is responsible for fatty acid uptake, and the reduced expression of acetyl CoA carboxylase-2 (*Acc2*), an enzyme that inhibits fatty acid oxidation and promotes fatty acid synthesis (Fig. 8).

Hepatic HAX-1 deficiency increases PDH activity

In view of the importance of the PDH complex in glucose oxidation, we determined PDH activities in livers of L-Hax1$^{+/+}$ and L-Hax1$^{-/-}$ mice and found that Hax-1 inactivation increased PDH activity in the liver (Fig. 9*A*). Whereas this increase was not due to changes in PDH kinase

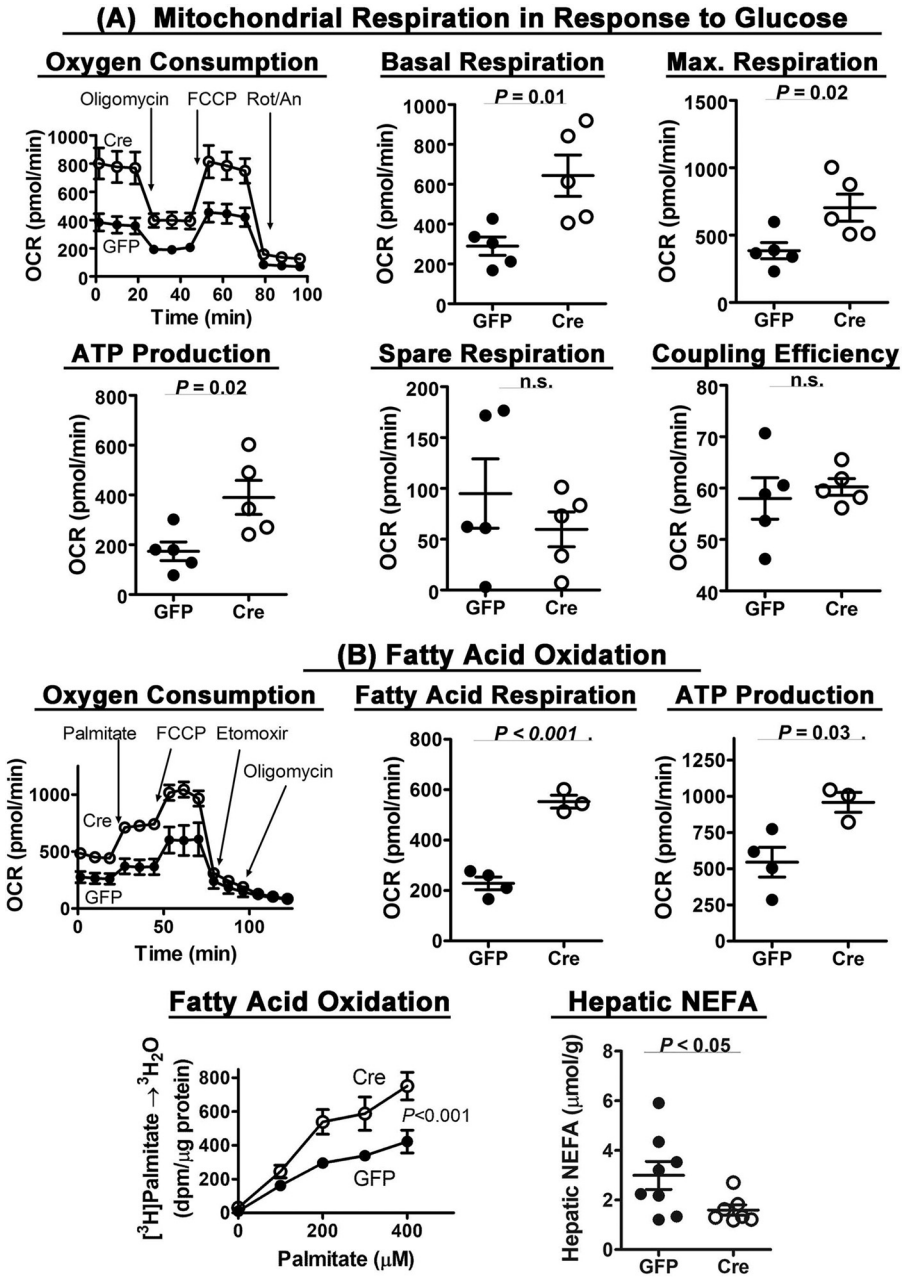

Figure 7. Hepatic HAX-1 deficiency increases mitochondrial respiration and fatty acid oxidation. *A*, primary hepatocytes isolated from GFP-injected (*solid symbols*) or *Cre*-injected (*open symbols*) *Hax1*$^{flox/flox}$ mice ($n = 5$) were incubated in medium containing 25 mM glucose, 1 mM sodium pyruvate, and 4 mM Glutamax to determine basal oxygen consumption rates. Oligomycin, FCCP, and rotenone/antimycin were added to measure ATP production, maximum and spare respiration, and coupling efficiency. *B*, fatty acid oxidation was determined after incubation with 150 μM palmitate. Etomoxir (50 μM) was added to inhibit fatty acid oxidation to determine oxygen consumption rate and ATP production due to fatty acid stimulation. Fatty acid oxidation was also determined in primary hepatocytes by monitoring the conversion of [^{3}H]palmitate to ^3H_2O. Nonesterified fatty acid levels in the livers of GFP- and *Cre*-injected mice ($n = 7–8$) were determined enzymatically after extraction. *n.s.*, not significant; *error bars*, S.D.

2 and 4 (PDK2 and -4) expression (Fig. 9*B*), HAX-1 inactivation significantly reduced PDHE1α phosphorylation under both chow– and Western diet–fed conditions (Fig. 9*C*). Increased mitochondrial respiration due to higher PDH activity has also been reported to elevate LDL receptor expression in hepatocytes (35). Indeed, increased LDL receptor protein levels were observed in Western diet–fed L-Hax1$^{-/-}$ mice compared with those observed in control mice (Fig. 9*D*). The increased level of LDL receptor may partly account for the lower plasma lipid levels observed in L-Hax1$^{-/-}$ mice.

Hepatic HAX-1 inactivation improves ER-mitochondria calcium homeostasis via InsP3R1 reduction

Increased PDH activity due to higher levels of nonphosphorylated PDH in the absence of differences in PDK2 and PDK4 suggested that HAX-1 inactivation may increase the dephosphorylation of PDH, a process that is mediated by calcium-dependent phosphatases in the mitochondria (36). In view of emerging evidence showing that ER and calcium homeostasis is an important determinant of mitochondrial respiration and metabolic diseases (19, 20, 37), and HAX-1 is present in both

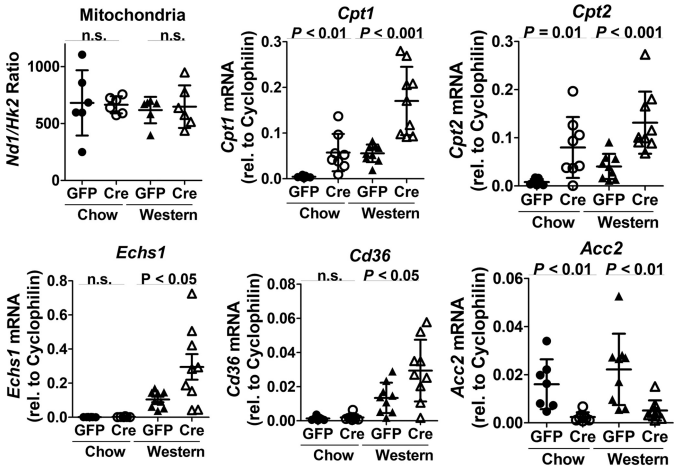

Figure 8. Hepatic HAX-1 inactivation increases expression of mitochondrial oxidation genes without changing mitochondria number. The relative mitochondria number was determined based on the ratio of the copy number of mitochondria gene *Nd1* to that of the nuclear gene *Hk2*. To determine expression of mitochondrial oxidation–related genes, total RNA was obtained from livers of chow-fed control (GFP, *solid bars*) and L-Hax1$^{-/-}$ (*Cre*, *open bars*) mice ($n = 5$) for quantitative RT-PCR quantification of mRNA. The data are reported as mean ± S.D. (*error bars*). Statistical significance was evaluated by two-tailed Student's *t* test between control and L-Hax1$^{-/-}$ mice under the same dietary conditions. *n.s.*, not significant.

the ER and the mitochondria, we determined whether HAX-1 inactivation influenced ER and mitochondria calcium homeostasis in the liver. Primary hepatocytes isolated from L-Hax1$^{-/-}$ mice were found to display significantly higher ER calcium levels compared with control mice under both normoglycemic (5 mM glucose) and hyperglycemic (25 mM glucose) conditions (Fig. 9*E*). In contrast, mitochondrial calcium levels were found to be lower in L-Hax1$^{-/-}$ hepatocytes compared with control cells (Fig. 9*F*). Importantly, HAX-1 inactivation also prevented palmitate- and hyperglycemia-induced mitochondrial calcium overload (Fig. 9*F*).

Mitochondrial dysfunction due to overnutrition is caused by excessive ER calcium transport to the mitochondria, a process that is mediated in part by InsP3R1 (37, 38). Interestingly, we found lower levels of InsP3R1 protein in the liver of L-Hax1$^{-/-}$ mice compared with control mice (Fig. 9*G*). To determine how HAX-1 may regulate InsP3R1 level in the liver, we performed co-immunoprecipitation experiments with HAX-1–specific antibodies and discovered that HAX-1 interacts with InsP3R1 (Fig. 9*G*). The finding that HAX-1 interacts with InsP3R1 and its ablation reduces InsP3R1 levels in hepatocytes is reminiscent of HAX-1's interaction with SERCA2 to suppress its degradation in the heart (30). Thus, the reduced InsP3R1 levels in L-Hax1$^{-/-}$ mice are likely due to its enhanced degradation. Importantly, the reduced InsP3R1 level due to HAX-1 deficiency limits ER calcium transport to the mitochondria, thereby preventing excessive nutrient-induced mitochondrial calcium overload and dysfunction.

Hepatic HAX-1 inactivation increases hepatic BSEP level and bile acid–responsive gene expression in intestine and liver

Another liver protein that interacts with HAX-1 and has activity that is sensitive to cellular calcium modulation is the bile salt export protein BSEP encoded by the *ABCB11* gene (33, 39). Consistent with results observed in kidney cells (33), BSEP levels in whole liver lysates as well as bile canalicular membranes were also higher in L-Hax1$^{-/-}$ mice compared with control mice (Fig. 10*A*). As described previously (40), the elevated BSEP expression also resulted in increased bile acid pool size, as reflected by higher levels of bile acids in plasma and liver (Fig. 10*B*). However, fecal bile acid levels and bile acid levels in the intestine were not different between these animals, suggesting that hepatic HAX-1 deficiency promotes the conservation of bile acids within the enterohepatic circulation, similar to that observed in liver-specific *Abcb11* transgenic mice (40, 41). Interestingly, we also observed increased excretion of cholesterol in the feces of both chow– and Western diet–fed L-Hax1$^{-/-}$ mice (Fig. 10*C*).

Similar to results reported for the *Abcb11* transgenic mice (40), hepatic HAX-1 deficiency did not alter intestinal expression of the bile acid transporter *Asbt* but robustly increased the expression of bile acid–responsive genes, including *Fgf15*, *Ostα/β*, and the short heterodimeric partner *Shp* (Fig. 11). The elevated bile acid pool size in L-Hax1$^{-/-}$ mice also led to farnesoid X receptor activation in the liver, as reflected by increased expression of *Shp*, *Abcg5*, and *Abcg8* (42) (Fig. 12). However, Cyp7a expression was found to be similar between control and L-Hax1$^{-/-}$ mice (Fig. 12). We also found that expression of sterol regulatory element-binding protein-1–responsive genes, which may be down-regulated by bile acids (43), were also lower, as reflected by reduced mRNA levels of acetyl-CoA carboxylase-1 (*Acc1*), fatty acid synthase (*Fasn*), and stearoyl-CoA desaturase (*Scd1*) in the livers of L-Hax1$^{-/-}$ mice (Fig. 12). Additionally, expression of the mitochondria cholesterol transport protein steroidogenic acute response protein (StAR) and the mitochondrial bile acid synthesis gene *Cyp27a* was also increased in the livers of Western diet-fed L-Hax1$^{-/-}$ mice (Fig. 12). The increased expression of *Abcg5* and *Abcg8* is consistent with higher fecal cholesterol content in L-Hax1$^{-/-}$ mice, whereas the increased expression of StAR, which mediates cholesterol transport into the mitochondria (44), and Cyp27a, which promotes the alternative acidic pathway of bile acid synthesis (45), may also partly account for the reduced hepatic cholesterol level and increased bile acid pool despite the decreased Cyp7a expression observed in L-Hax1$^{-/-}$ mice. Taken together, these data indicate that hepatic HAX-1 inactivation, via increased BSEP levels in bile canaliculus membrane and enterohepatic bile acid circulation (40), also protects against diet-induced metabolic disease by activation of bile acid–responsive genes in the intestine and liver.

Discussion

The current study presents the first evidence that hepatic HAX-1 inactivation in male mice increases insulin sensitivity and protects against diet-induced hyperlipidemia, hyperinsulinemia, and hepatosteatosis. This study did not examine female mice; thus, metabolic benefits of HAX-1 inactivation in females remain uncertain. Nevertheless, the impact of HAX-1 inactivation in male mice is highly potent, as low insulin concentration is sufficient to maintain euglycemia in chow-fed L-Hax1$^{-/-}$ mice.

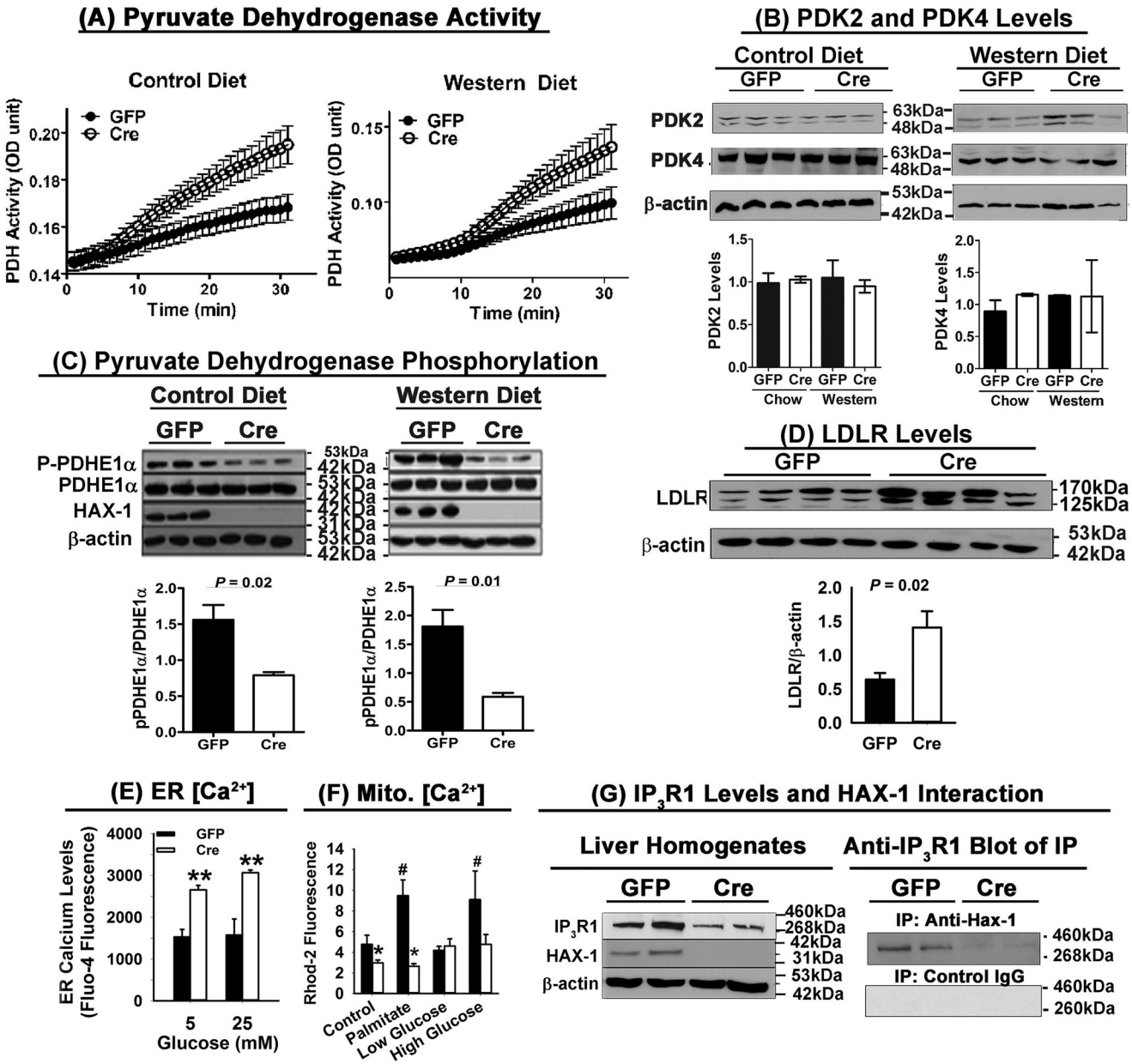

Figure 9. Hepatic HAX-1 inactivation increased pyruvate dehydrogenase activity and reduced phosphorylation with a corresponding increase in LDL receptor (*LDLR*) levels in mechanisms related to improvement of ER and mitochondria calcium homeostasis. *A*, liver homogenates prepared from control and Western diet–fed control (GFP-injected) and L-Hax1$^{-/-}$ (*Cre*-injected) mice ($n = 6$) were used to measure PDH enzymatic activity. Western blot analyses were performed with the lysates with antibodies against PDK2 and PDK4 (*B*) and antibodies against PDH-E1α and antibodies specific to PDH-E1α phosphorylated at residue Ser-300 (*C*). PDH phosphorylation was determined based on the ratio of pPDHE1α/PDHE1α intensity in each sample. The data represent mean ± S.D. (*error bars*) from three biological replicates. *D*, the liver homogenates were also subjected to Western blot analysis with antibodies against the LDL receptor, with anti-β-actin blots used as loading controls. The data represent mean ± S.D. from four biological replicates. *E*, hepatocytes isolated from control (GFP, *solid bars*) and HAX-1–inactivated (*Cre*, *open bars*) mice were incubated with 5 or 25 mM glucose. Thapsigargin was added to induce Ca^{2+} release. Relative ER [Ca^{2+}] was determined by Fluo-4 fluorescence. The data represent mean ± S.D. from $n = 4$ mice in each group. **, $p < 0.01$ compared with control as evaluated by Student's *t* test. *F*, hepatocytes isolated from control (GFP, *solid bars*) and HAX-1–inactivated (*Cre*, *open bars*) mice were incubated with buffer with or without 150 μM palmitate or with 5 or 25 mM glucose. Mitochondrial calcium levels were measured by the mitochondria-specific fluorescence indicator Rhod-2. The data represent mean ± S.D. from $n = 4$ mice in each group. *, $p < 0.01$ compared with GFP hepatocytes; #, $p < 0.01$ compared with control without addition as evaluated by Student's *t* test. *G*, liver homogenates from chow-fed control (GFP) and L-Hax1$^{-/-}$ (*Cre*) mice were immunoprecipitated with anti-HAX-1 antibodies ($n = 4$ in each group). Representative Western blots show total liver lysates and the anti-HAX-1 immunoprecipitated IP_3R1 using β-actin immunoreactivity as loading control.

The metabolic benefits of hepatic HAX-1 inactivation are multifactorial due to (i) reduction of InsP3R1 levels to maintain ER-mitochondria calcium homeostasis, thereby preventing excess nutrient-induced mitochondria calcium overload and dysfunction; (ii) decreased PDH phosphorylation, thereby improving mitochondrial respiration to increase nutrient utilization and LDL receptor expression to enhance postprandial lipid clearance; and (iii) increased BSEP levels and its presence in the bile canaliculus membrane, thereby improving enterohepatic bile acid circulation, which leads to activation of bile acid–responsive genes in intestine and liver to augment insulin sensitivity and reduce hepatic cholesterol levels. The improvement

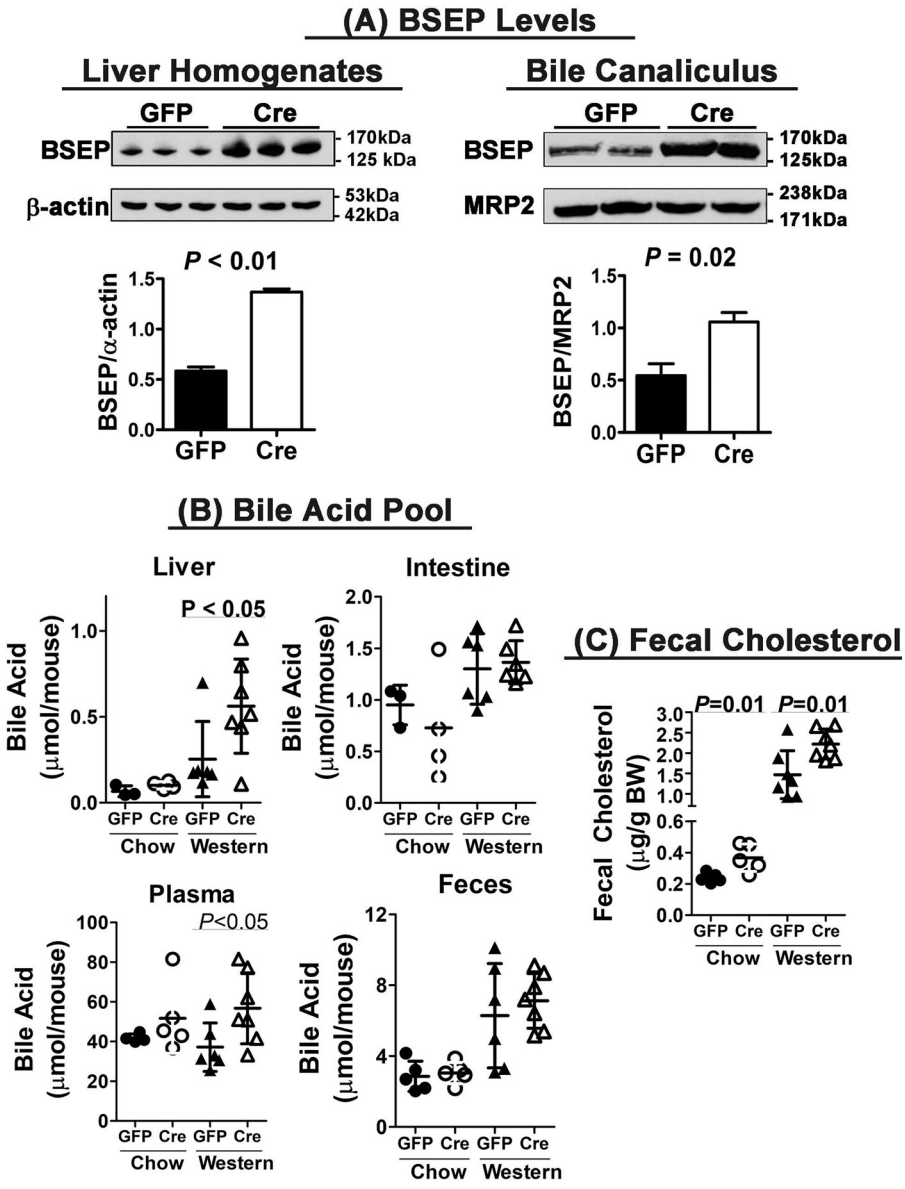

Figure 10. Hepatic HAX-1 inactivation increases liver BSEP/ABCB11 levels, bile acid pool size, and fecal cholesterol content. *A*, representative Western blots of $n = 3$ experiments showing BSEP levels in total liver homogenates and bile canaliculus membranes from chow-fed control (GFP) and L-Hax1$^{-/-}$ (*Cre*) mice. β-Actin and MRP2 immunoreactivities were used as loading controls for liver homogenates and bile canaliculus membrane preparations, respectively. Differences of band intensity after normalization with loading controls were evaluated by Student's *t* test. *B*, bile acid levels were determined in various tissues and plasma from chow-fed ($n = 4$) and Western diet–fed ($n = 7$) GFP- and *Cre*-injected *Hax1*$^{flox/flox}$ mice. *C*, feces collected from seven mice in each group were extracted for lipids to determine fecal cholesterol levels. *Error bars*, S.D.

of bile acid recycling also results in suppression of SREBP-1–responsive genes in the liver, leading to reduced lipogenesis, as well as increased expression of mitochondrial oxidation genes, probably due to bile acid–induced expression of these peroxisome proliferator–activated receptor α genes (46).

It is interesting to note that despite their improvement in hepatic mitochondrial respiration and fatty acid oxidation, Western diet–fed L-Hax1$^{-/-}$ mice displayed similar body weight gain and adiposity as control mice. This apparent paradox may be due to a slight increase in food intake as well as the reduced adipocyte lipolysis in Western diet–fed L-Hax1$^{-/-}$ mice, as indicated by their lower fasting plasma NEFA levels compared with control mice (Fig. 4*E*). The reduced adipocyte lipolysis in Western diet–fed L-Hax1$^{-/-}$ mice may be related to their improved insulin sensitivity (Fig. 4*D*) (47). This hypothesis relating hepatic nutrient oxidation with insulin sensitivity and adipocyte lipolysis will require more direct experimentation before any definitive conclusions can be made.

Our data revealed that HAX-1 interacts with InsP3R1 and that its ablation reduces InsP3R1 in hepatocytes, which is reminiscent of HAX-1 regulation of SERCA2a degradation in the heart (30). Although InsP3R1 signaling is necessary for ER calcium release to the mitochondria to sustain cellular bioenergetics and its total absence diminishes PDH complex activity due to impairment of calcium-dependent dephosphorylation (48), excessive ER calcium transport to the mitochondria also causes mitochondrial dysfunction especially under overnutrition conditions (37, 38). Thus, exquisite control of InsP3R1 level/activ-

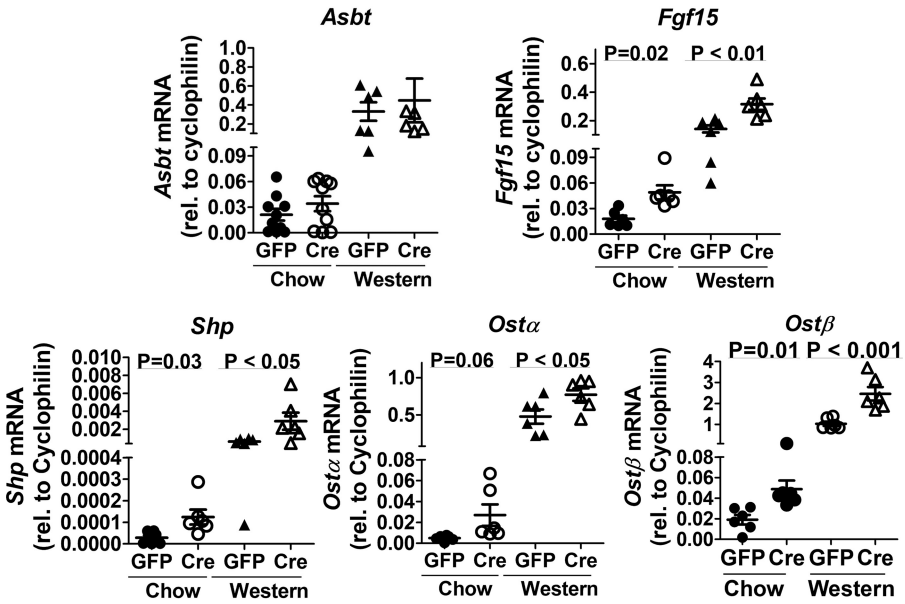

Figure 11. Hepatic HAX-1 inactivation increases the expression of bile acid–responsive genes in the intestine. Expression of bile acid transporter Asbt and other bile acid–responsive genes, including *Fgf15, Shp*, and *Ostα/β*, in the intestinal ileum was measured by quantitative RT-PCR quantification of total RNA extracted from six control and six L-Hax1$^{-/-}$ mice. The data represent mean ± S.D. (*error bars*). Statistical evaluation comparing mice with different genotype on the same diet was performed using Student's *t* test.

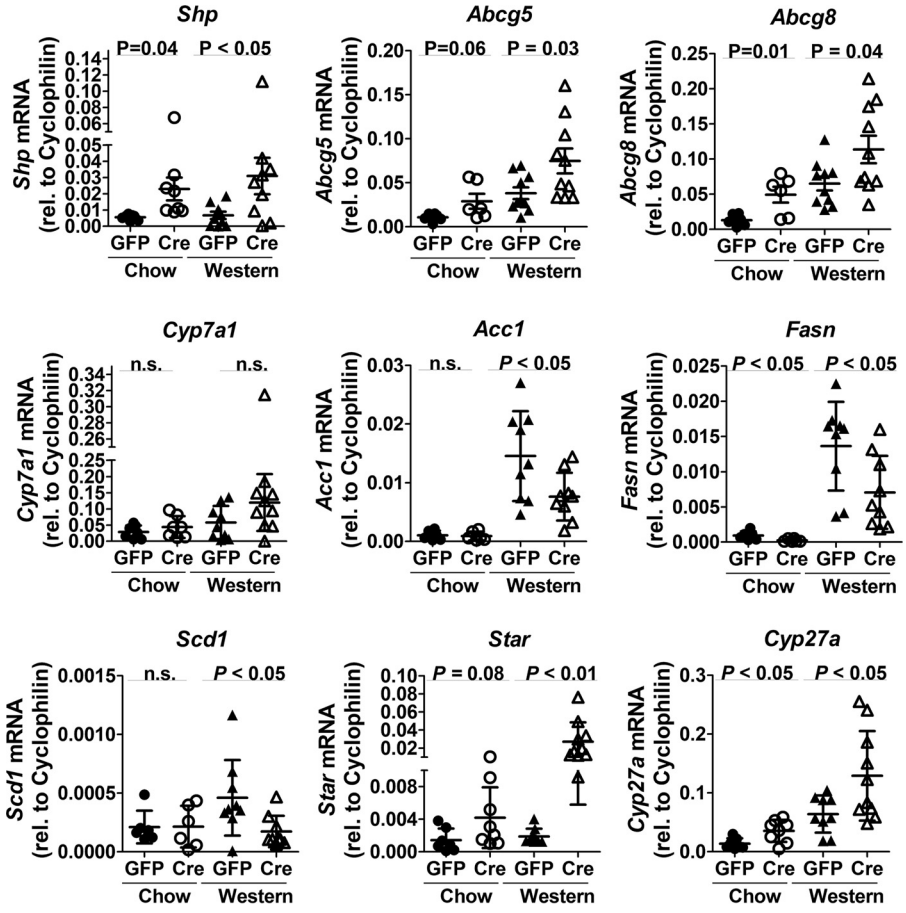

Figure 12. Hepatic HAX-1 inactivation activates FXR and reduces SREBP-1 genes in liver. Six control and 8–9 L-Hax1$^{-/-}$ mice were used to measure hepatic expression of FXR-responsive genes, such as *Shp, Abcg5*, and *Abcg8*, and SREBP-1–responsive genes, such as *Acc1*, *Fasn*, and *Scd1*. The RNA was also used for quantitative PCR to measure expression of alternative bile acid pathway genes, such as *Star*, and *Cyp27a*. The data represent mean ± S.D. (*error bars*). Statistical evaluation comparing mice with different genotypes on the same diet was performed by Student's *t* test.

ity is necessary to optimize metabolic homeostasis. In the current study, we showed that HAX-1 inactivation lowers but does not ablate InsP3R1 expression, thereby leading to the prevention of mitochondrial calcium overload, decreased PDH phosphorylation, and improvement of mitochondrial activity in hepatocytes. These results are consistent with previous reports that silencing of InsP3R1 improves mitochondrial activity and maintains metabolic homeostasis in obese mice (37). Liver-specific InsP3R1 inactivation also reduces lipid droplet formation and protects against high-fat diet–induced hepatosteatosis (49). Additionally, our results showed that increased glucose oxidation also lowers postprandial VLDL secretion. This observation, along with increased hepatic LDL receptor expression due to higher PDH activity (35), may explain the resistance of L-Hax1$^{-/-}$ mice to diet-induced hyperlipidemia. Taken together, these results indicate that PDH activation via InsP3R1 reduction is one mechanism by which L-Hax1$^{-/-}$ mice were protected against Western diet–induced hyperinsulinemia, hyperlipidemia, and hepatosteatosis.

The importance of PDH activity in mitochondrial respiration is well-established in the literature. As noted above, PDH activity is inactivated by phosphorylation with PDKs and can be activated by PDH phosphatase–mediated dephosphorylation. Inactivation of the major PDK enzymes in the liver has been shown to be protective against diet-induced glucose intolerance and hepatosteatosis (50, 51). These and other similar studies suggested that hepatic PDK enzymes may be therapeutic targets for diabetes management, and indeed a liver-specific pan-PDK inhibitor was effective in improving insulin signaling and lowers hepatic lipid accumulation in high-fat diet–induced obese mice (52). Nevertheless, despite these encouraging results, it is noteworthy that normalization of plasma glucose and insulin levels as well as the amelioration of hepatosteatosis were not achieved in these animal models. Hence, additional approaches to complement PDH activation may be necessary for optimal metabolic benefits.

The current study showed that normal plasma glucose, insulin, and lipid levels can be achieved in Western diet–fed mice by liver-specific inactivation of HAX-1. Hepatosteatosis was also significantly reduced in Western diet–fed L-Hax1$^{-/-}$ mice compared with control mice. In addition to reducing PDH phosphorylation and improving mitochondrial activity, HAX-1 inactivation in the liver also increased BSEP/ABCB11 levels and its localization to the bile canaliculus. This result is consistent with a previous study reporting that HAX-1 interacts with BSEP/ABCB11 and that the absence of HAX-1 increases BSEP/ABCB11 localization to the apical membranes of liver and kidney cells (33). Although the exact mechanism underlying the increased BSEP/ABCB11 remains unknown, it is tempting to speculate that the reduced expression of InsP3R1 redirects InsP3 to InsP3R2, which has been shown previously to promote BSEP/ABCB11 translocation and bile salt export activity (39). This hypothesis will be examined more rigorously in future studies. More importantly, elevated BSEP/ABCB11 has also been shown to enhance enterohepatic cycling of bile salts without significant change in fecal bile salt excretion (41).

Taken together, our results indicate that hepatic HAX-1 inactivation mimics bariatric surgery with respect to enhancing bile salt recycling through the enterohepatic circulation and increased expression of FGF15 and other bile acid–responsive genes in intestine. FGF15 and its human ortholog FGF19 are incretins secreted by the intestine and regulate glucose homeostasis by improving insulin sensitivity in hepatic and extrahepatic tissues (53). The observation that less insulin is required to maintain euglycemia in chow-fed L-Hax1$^{-/-}$ mice and their protection against Western diet–induced hyperinsulinemia is consistent with the interpretation that metabolic benefits of hepatic HAX-1 inactivation are at least in part due to increased BSEP/ABCB11-mediated FGF15 expression in the intestine. However, despite these benefits of elevated hepatic BSEP/ABCB11 levels to increase bile acid recirculation, its overexpression in the liver alone may be compromised due to an indirect effect of increasing cholesterol absorption through the intestine (54). Thus, a strategy to promote postprandial lipid clearance is necessary to complement the BSEP/ABCB11 increase for optimal metabolic benefits. In this regard, the present study shows that hepatic HAX-1 inactivation reduces postprandial VLDL secretion and increases LDL receptor expression in the liver, indicating that targeting hepatic HAX-1 may hold therapeutic promise along these lines.

Experimental procedures

Antibodies, primers, and key reagents

All antibodies and primers used in the current study were obtained commercially as listed in Tables S1 and S2.

Animals

All animal experimental protocols were reviewed and approved by the institutional animal care and use committee at the University of Cincinnati (approval 17-09-08-01) in accordance with the Guide for the Care and Use of Laboratory Animals of the National Institutes of Health. The *Hax1*$^{flox/flox}$ mice generated originally in the Ihle laboratory (55) were mated with C57BL/6J mice for 6 generations to establish a colony of *Hax1*$^{flox/flox}$ mice. Liver-specific *Hax1* knockout (L-Hax1$^{-/-}$) mice were developed by injecting the *Hax1*$^{flox/flox}$ mice with 5×10^{11} genome copies of adeno-associated virus (AAV) expressing the *Cre* recombinase gene under the control of the liver-specific TBG promoter (AAV-TBG-*Cre*). The *Hax1*$^{flox/flox}$ mice injected with AAV-TBG-GFP were used as a control without HAX-1 deletion. Male *Hax1*$^{flox/flox}$ littermates at the age of 10 weeks were used for AAV injection. Mice were fed either a normal chow diet (Teklad, Madison, WI) or a Western type diet containing 15.2% kcal protein, 42.7% kcal carbohydrate, 42.0% kcal fat, and 0.2% cholesterol (Teklad, TD88137). Animal characterization was performed after an overnight fast, typically after a 12-week dietary period. Body weights were determined using a Denver 300K scale, and adiposity measurements were obtained using ^{1}H magnetic resonance spectroscopy (EchoMRI-100, Echomedical Systems, Houston, TX) as described previously (56).

Blood chemistry

Blood was collected from mice after an overnight fast. Blood glucose levels were measured using an Accu-Check Active Glu-

cometer. Plasma insulin levels were determined by ELISA kits. Plasma cholesterol and triglycerides were determined using Infinity cholesterol and triglyceride kits (Table S1). Plasma nonesterified fatty acid levels were measured using calorimetric assay kits (Wako Chemicals, Richmond, VA). For lipoprotein separation, 200 μl of plasma pooled from 4–5 mice in each group were subjected to fast-performance liquid chromatography (FPLC) on two Superose 6 HR 10/30 columns connected in tandem (Amersham Biosciences), and 0.5-ml fractions were collected for cholesterol and triglyceride determinations. For the glucose tolerance test, a glucose solution (2 g/kg body weight) was administered by oral gavage after an overnight fast, and blood glucose levels were measured over a 2-h period. For the insulin tolerance test, blood glucose levels in fasted mice were monitored over a 90-min period after intraperitoneal insulin injection (0.75 units/kg body weight).

Histology

Tissues were fixed in 4% paraformaldehyde overnight, dehydrated, and then embedded in paraffin to prepare 5-μm sections. The sections were stained with hematoxylin and eosin and visualized under a light microscope.

Lipid accumulation in liver

Liver tissue was homogenized in buffer containing 50 mM Tris-HCl, pH 7.4, 150 mM NaCl, and 5 mM EDTA (0.5 g/ml) in the presence of 0.5 μCi of [^{3}H]cholesterol for extraction efficiency. The lipids were extracted twice with 1 ml of petroleum ether, mixed, and centrifuged at 1000 $\times$ *g* for 10 min. Fifty μl of the organic phase was collected, dried, and used to quantify triglyceride, cholesterol, and NEFA levels in each sample. Extraction efficiency was normalized based on recovery of the [^{3}H]cholesterol.

Hepatic triglyceride secretion and de novo lipogenesis

After an overnight fast, mice were injected intraperitoneally with a 10% solution of Poloxamer 407 (1 g/kg body weight) diluted in saline to assess triglyceride secretion. Postprandial lipid clearance was performed by administering a 200-μl bolus of olive oil to each animal by oral gavage. For both experiments, blood samples (50 μl) were collected from the tail vein prior to and hourly thereafter to measure triglyceride levels. For *in vitro* studies, primary hepatocytes, isolated as described previously (57), were incubated in serum-free M199 medium for 24 h either in nonstimulated medium (5 mM glucose and 0.1 μM dexamethasone) or stimulated medium (25 mM glucose with 100 nM insulin and 0.1 μM dexamethasone). Lipids were extracted from the media and cell lysates with chloroform/methanol (2:1, v/v) for the triglyceride assay. The hepatocytes were also stained with Oil Red O to visualize lipid accumulation under a microscope. Lipogenesis *in vivo* was performed by feeding a [^{14}C]glucose solution (2 mg/g, 0.05 μCi) by intragastric gavage. Tissues were harvested after 2 h for lipid extraction with chloroform/methanol (2:1). The rate of glucose incorporation into newly synthesized fatty acids was calculated as nmol of [^{14}C]glucose incorporated into fatty acids/g of tissue.

Pyruvate dehydrogenase activity measurement

Lysates were prepared from the livers of GFP- and *Cre*-injected *Hax1*$^{flox/flox}$ mice by homogenization in ice-cold PBS containing protease inhibitor mixture (Roche Diagnostics). Four hundred μg of protein in each lysate was used to measure PDH enzymatic activity using a commercially available kit (Table S1).

Cellular oxygen consumption and fatty acid oxidation

Oxygen consumption rate (OCR) was measured in intact hepatocytes in real time using an XF24 Extracellular Flux Analyzer and the XF 24 version 1.5.0.69 software. Hepatocytes were seeded on collagen-coated XF24 plates at 10,000 cells/well. The cells were incubated for 1 h at ambient temperature and then overnight at 37 °C in William's E medium supplemented with 100 units/ml penicillin/streptomycin, 2 mM L-glutamine, 5% FBS, 100 nM insulin, and 100 nM dexamethasone. The cells were rinsed twice with PBS and kept at 37 °C in 500 μl of Dulbecco's modified Eagle's medium supplemented with 25 mM glucose, 1 mM sodium pyruvate, and 4 mM Glutamax for 1 h in a CO_2-free incubator in the Seahorse Extracellular Flux Analyzer. After baseline measurement, additions were delivered in the following order through the instrument's individual injection ports: oligomycin (12 μg/ml), FCCP (1.5 μM), and rotenone (1 μM)/antimycin A (1.5 μM) (Sigma).

For fatty acid oxidation, cells were incubated for 5 h in Dulbecco's modified Eagle's medium without any substrate, washed with Krebs–Henseleit buffer (11 mM NaCl, 4.7 mM KCl, 2 mM $MgSO_4$, 1.2 mM Na_2HPO_4, 2.5 mM glucose, 0.5 mM carnitine, and 0.1 μM insulin), and then incubated with 500 μl of the same buffer in a CO_2-free incubator at 37 °C for 1 h. BSA-conjugated palmitate (150 μM) was added to stimulate oxygen consumption. Etomoxir was added in port B to a final concentration of 50 μM on the flux plate to inhibit respiration and to calculate fatty acid–specific OCR and ATP production rate.

Fatty acid oxidation in hepatocytes was also assessed by measuring the release of ^3H_2O after incubation of hepatocytes with [9,10-^{3}H]palmitic acid as described (58). Briefly, the hepatocytes were incubated with 0–400 μM BSA-conjugated [^{3}H]palmitate and 0.5 mM carnitine for 2 h at 37 °C. The medium was removed, and the proteins were precipitated with TCA and then neutralized with NaOH. The ^3H_2O in the supernatant was extracted by Dowex 1X8 resin (Sigma) for scintillation counting. The amount of ^3H_2O released was normalized to the amount of proteins in the cell lysate.

Calcium measurements

Changes in intracellular calcium concentrations in hepatocytes were determined using the Fluo-4 AM NW calcium assay kit. Following culture of cells with serum-free M119 medium for 16 h in the presence of 5 or 25 mM glucose, the hepatocytes were loaded with Fluo-4 AM in the presence of probenecid. Thapsigargin (450 nM) or DMSO was added, and fluorescence (490-nm excitation; 516-nm emission) was measured over a 5-min period. Calcium levels in the ER are expressed as fluorescence units in thapsigargin-treated cells minus fluorescence units in DMSO-treated cells. Mitochondrial calcium levels under basal and nutrient-stimulated conditions were assessed

as described (38). In brief, the hepatocytes were incubated with or without 150 μM palmitate or with 5 or 25 mM glucose for 6 h prior to the addition of the mitochondria-specific calcium indicator Rhod-2 AM. The cells were washed three times and then replenished with fresh medium to measure fluorescence intensity (552-nm excitation; 581-nm emission).

Fecal cholesterol measurements

Feces were collected from individually housed mice over 3 days. Dried feces (0.3–0.5 g) were then minced and extracted in 2.5 ml of saline and 2.5 ml of chloroform/methanol (2:1, v/v). The organic phase that contains the extracted lipids was collected in a glass tube, air-dried, and then redissolved in 400 μl of 100% ethanol, and cholesterol content was measured enzymatically using a cholesterol assay kit (Table S1).

Bile acid analysis

Bile acid levels in plasma, liver, small intestine, and feces were measured as described (57). Briefly, fasting mice were sacrificed, and fresh tissues were collected, weighed, and minced. Bile acids were extracted with 75% ethanol for 1 h at 50 °C. Bile acids were measured enzymatically using the mouse total bile acid assay kit (Table S1). Bile acid levels in each tissue were expressed as μmol/kg body weight of each animal.

Co-immunoprecipitation

The HAX-1–specific antibodies were cross-linked to Protein A Dynabeads with BS3 cross-linker prior to incubation for 12 h at 4 °C with liver lysates that had been precleared with off-target antibody and Protein A–Sepharose beads. The samples were eluted with 2× NuPAGE lithium dodecyl sulfate sample buffer (Table S1) for 5 min at 95 °C and used for Western blot analysis.

Western blot analysis

Livers were excised and homogenized in ice-cold radioimmune precipitation assay buffer containing protease and phosphatase inhibitor mixture. For assessment of BSEP expression, canalicular plasma membrane was isolated as described previously (59). Samples were diluted with a 4× volume of SDS sample buffer (40% (v/v) glycerol, 240 mM Tris-HCl (pH 6.8), 8% SDS, 0.04% bromphenol blue, 5% β-mercaptoethanol) and heated at 95 °C for 5 min. The samples were electrophoresed on Express Plus PAGE gels and then transferred to polyvinylidene difluoride membranes. The membranes were blocked in TBS solution containing 5% milk and 0.1% Tween 20 for 1 h at 4 °C and then incubated for 90 min with a 1:1000 dilution of primary antibodies. The membranes were washed and then incubated with horseradish peroxidase–conjugated secondary antibodies and visualized using Pierce enhanced chemiluminescence reagents.

Real-time PCR analysis to determine mitochondria number and gene expression

Total genomic DNA was extracted from 30 mg of liver tissues using the DNeasy blood and tissue kit (Qiagen, CA). Relative mitochondrial DNA copy number was determined by quantitative PCR utilizing the mitochondrial NADH dehydrogenase 1 (ND1) gene as a marker for mitochondrial DNA and hexokinase 2 (HK2) as a marker for the nuclearly encoded gene. To determine gene expression, RNA was extracted from tissues using Direct-Zol RNA kits and then used to generate cDNA using the qScript cDNA synthesis kit. Quantitative real-time PCR was performed on a StepOnePlus Fast thermocycler using Fast SYBR Green master mix with primer sequences as shown in Table S2.

Statistical analysis

Sample size for each experiment was estimated based on previous studies documenting that 6 mice/group are sufficient to evaluate statistically significant differences in diet-induced body weight gains, adiposity, and plasma lipid, glucose, and insulin levels (60). Mice were not randomized prior to assignment to experimental groups. No samples, mice, or data points were excluded from the reported analyses. Statistical analysis was performed using SigmaPlot version 13.0 software. Normality was examined using the Shapiro–Wilk test. Data with equal variance based on Brown–Forsythe analysis were evaluated by Student's t test for studies comparing two groups. Data with unequal variance were evaluated using the Mann–Whitney test. Differences at $p < 0.05$ were considered statistically significant.

Author contributions—F. A., S. C., A. J., and D. Y. H. data curation; F. A., S. C., A. J., E. G. K., and D. Y. H. formal analysis; F. A., S. C., A. J., E. G. K., and D. Y. H. investigation; F. A., A. J., and E. G. K. methodology; F. A. writing-original draft; S. C. and D. Y. H. validation; S. C., A. J., and D. Y. H. writing-review and editing; A. J., E. G. K., and D. Y. H. conceptualization; A. J., E. G. K., and D. Y. H. supervision; D. Y. H. resources; D. Y. H. funding acquisition; D. Y. H. project administration.

Acknowledgments—We thank Eddy Konaniah for technical assistance with histology and April Haller for assistance with animal breeding and maintenance.

References

1. Day, C. P. (2011) Non-alcoholic fatty liver disease: a massive problem. *Clin. Med.* (*Lond.*) **11,** 176–178 CrossRef Medline
2. Kneeman, J. M., Misdraji, J., and Corey, K. E. (2012) Secondary causes of nonalcoholic fatty liver disease. *Therap. Adv. Gastroenterol.* **5,** 199–207 CrossRef Medline
3. Goh, G. B.-B., Pagadala, M. R., Dasarathy, J., Unalp-Arida, A., Sargent, R., Hawkins, C., Sourianarayanane, A., Khiyami, A., Yerian, L., Pai, R. K., Dasarathy, S., and McCullough, A. J. (2015) Clinical spectrum of non-alcoholic fatty liver disease in diabetic and non-diabetic patients. *BBA Clin.* **3,** 141–145 CrossRef Medline
4. Delea, T. E., Edelsberg, J. S., Hagiwara, M., Oster, G., and Phillips, L. S. (2003) Use of thiazolidinediones and risk of heart failure in people with type 2 diabetes: a retrospective cohort study. *Diabetes Care* **26,** 2983–2989 CrossRef Medline
5. Amori, R. E., Lau, J., and Pittas, A. G. (2007) Efficacy and safety of incretin therapy in type 2 diabetes: systematic review and meta-analysis. *JAMA* **298,** 194–206 CrossRef Medline
6. Triplitt, C., McGill, J. B., Porte, D., and Conner, C. S. (2007) The changing landscape of type 2 diabetes: the role of incretin-based therapies in managed care outcomes. *J. Manag. Care Pharm.* **13,** S2–S16 CrossRef Medline
7. Bain, S. C., and Stephens, J. W. (2008) Exenatide and pancreatitis: an update. *Expert Opin. Drug Saf.* **7,** 643–644 CrossRef Medline

8. Kaushal, S., Singh, H., Thangaraju, P., and Singh, J. (2014) Canagliflozin: a novel SGLT2 inhibitor for type 2 diabetes mellitus. *N. Am. J. Med. Sci.* **6,** 107–113 CrossRef Medline
9. Polonsky, K. S., and Klein, S. (2008) Gastric banding to treat obesity: band-aid or breakthrough. *Nat. Clin. Pract. Endocrinol. Metab.* **4,** 421 CrossRef Medline
10. Ahmad, N. N., Pfalzer, A., and Kaplan, L. M. (2013) Roux-en-Y gastric bypass normalizes the blunted postprandial bile acid excursion associated with obesity. *Int. J. Obes.* (*Lond.*) **37,** 1553–1559 CrossRef Medline
11. Patti, M. E., Houten, S. M., Bianco, A. C., Bernier, R., Larsen, P. R., Holst, J. J., Badman, M. K., Maratos-Flier, E., Mun, E. C., Pihlajamaki, J., Auwerx, J., and Goldfine, A. B. (2009) Serum bile acids are higher in humans with prior gastric bypass: potential contribution to improved glucose and lipid metabolism. *Obesity* **17,** 1671–1677 CrossRef Medline
12. Nakatani, H., Kasama, K., Oshiro, T., Watanabe, M., Hirose, H., and Itoh, H. (2009) Serum bile acid along with plasma incretins and serum high-molecular weight adiponectin levels are increased after bariatric surgery. *Metabolism* **58,** 1400–1407 CrossRef Medline
13. Kohli, R., Bradley, D., Setchell, K. D., Eagon, J. C., Abumrad, N., and Klein, S. (2013) Weight loss induced by Roux-en-Y gastric bypass but not laparoscopic adjustable gastric banding increases circulating bile acids. *J. Clin. Endocrinol. Metab.* **98,** E708–E712 CrossRef Medline
14. Myronovych, A., Kirby, M., Ryan, K. K., Zhang, W., Jha, P., Setchell, K. D., Dexheimer, P. J., Aronow, B., Seeley, R. J., and Kohli, R. (2014) Vertical sleeve gastrectomy reduces hepatic steatosis while increasing serum bile acids in a weight-loss-independent manner. *Obesity* **22,** 390–400 CrossRef Medline
15. Thomas, C., Gioiello, A., Noriega, L., Strehle, A., Oury, J., Rizzo, G., Macchiarulo, A., Yamamoto, H., Mataki, C., Pruzanski, M., Pellicciari, R., Auwerx, J., and Schoonjans, K. (2009) TGR5-mediated bile acid sensing controls glucose homeostasis. *Cell Metab.* **10,** 167–177 CrossRef Medline
16. Inagaki, T., Choi, M., Moschetta, A., Peng, L., Cummins, C. L., McDonald, J. G., Luo, G., Jones, S. A., Goodwin, B., Richardson, J. A., Gerard, R. D., Repa, J. J., Mangelsdorf, D. J., and Kliewer, S. A. (2005) Fibroblast growth factor 15 functions as an enterohepatic signal to regulate bile acid homeostasis. *Cell Metab.* **2,** 217–225 CrossRef Medline
17. Schumacher, J. D., Kong, B., Pan, Y., Zhan, L., Sun, R., Aa, J., Rizzolo, D., Richardson, J. R., Chen, A., Goedken, M., Aleksunes, L. M., Laskin, D. L., and Guo, G. L. (2017) The effect of fibroblast growth factor 15 deficiency on the development of high fat diet-induced non-alcoholic steatohepatitis. *Toxicol. Appl. Pharmacol.* **330,** 1–8 CrossRef Medline
18. Chella Krishnan, K., Kurt, Z., Barrere-Cain, R., Sabir, S., Das, A., Floyd, R., Vergnes, L., Zhao, Y., Che, N., Charugundla, S., Qi, H., Zhou, Z., Meng, Y., Pan, C., Seldin, M. M., *et al.* (2018) Integration of multi-omics data from mouse diversity panel highlights mitochondrial dysfunction in non-alcoholic fatty liver disease. *Cell Syst.* **6,** 103–115.e7 CrossRef Medline
19. Rieusset, J. (2017) Endoplasmic reticulum-mitochondria calcium signaling in hepatic metabolic diseases. *Biochim. Biophys. Acta Mol. Cell Res.* **1864,** 865–876 CrossRef Medline
20. Arruda, A. P., and Hotamisligil, G. S. (2015) Calcium homeostasis and organelle function in the pathogenesis of obesity and diabetes. *Cell Metab.* **22,** 381–397 CrossRef Medline
21. Park, S. W., Zhou, Y., Lee, J., Lee, J., and Ozcan, U. (2010) Sarco(endo)plasmic reticulum Ca^{2+}-ATPase 2b is a major regulator of endoplasmic reticulum stress and glucose homeostasis in obesity. *Proc. Natl. Acad. Sci. U.S.A.* **107,** 19320–19325 CrossRef Medline
22. Wang, Y., Li, G., Goode, J., Paz, J. C., Ouyang, K., Screaton, R., Fischer, W. H., Chen, J., Tabas, I., and Montminy, M. (2012) Inositol-1,4,5-trisphosphate receptor regulates hepatic gluconeogenesis in fasting and diabetes. *Nature* **485,** 128–132 CrossRef Medline
23. Feriod, C. N., Oliveira, A. G., Guerra, M. T., Nguyen, L., Richards, K. M., Jurczak, M. J., Ruan, H.-B., Camporez, J. P., Yang, X., Shulman, G. I., Bennett, A. M., Nathanson, M. H., and Ehrlich, B. E. (2017) Hepatic inositol 1,4,5 trisphosphate receptor type 1 mediates fatty liver. *Hepatol. Commun.* **1,** 23–35 CrossRef Medline
24. Hippe, A., Bylaite, M., Chen, M., von Mikecz, A., Wolf, R., Ruzicka, T., and Walz, M. (2006) Expression and tissue distribution of mouse Hax1. *Gene* **379,** 116–126 CrossRef Medline
25. Fadeel, B., and Grzybowska, E. (2009) HAX-1: a multifunctional protein with emerging roles in human disease. *Biochim. Biophys. Acta* **1790,** 1139–1148 CrossRef Medline
26. Yap, S. V., Vafiadaki, E., Strong, J., and Kontrogianni-Konstantopoulos, A. (2010) HAX-1: a multifaceted antiapoptotic protein localizing in the mitochondria and the sarcoplasmic reticulum of striated muscle cells. *J. Mol. Cell. Cardiol.* **48,** 1266–1279 CrossRef Medline
27. Simmen, T. (2011) HAX-1: a regulator of calcium signaling and apoptosis progression with multiple roles in human disease. *Expert Opin. Ther. Targets* **15,** 741–751 CrossRef Medline
28. Han, J., Goldstein, L. A., Hou, W., Froelich, C. J., Watkins, S. C., and Rabinowich, H. (2010) Deregulation of mitochondrial membrane potential by mitochondrial insertion of granzyme B and direct HAX-1 cleavage. *J. Biol. Chem.* **285,** 22461–22472 CrossRef Medline
29. Zhao, W., Waggoner, J. R., Zhang, Z.-G., Lam, C. K., Han, P., Qian, P., Qian, J., Schroder, P. M., Mitton, B., Kontrogianni-Konstantopoulos, A., Robia, S. L., and Kranias, E. G. (2009) The anti-apoptotic protein HAX-1 is a regulator of cardiac function. *Proc. Natl. Acad. Sci. U.S.A.* **106,** 20776–20781 CrossRef Medline
30. Bidwell, P. A., Liu, G.-S., Nagarajan, N., Lam, C. K., Haghighi, K., Gardner, G., Cai, W.-F., Zhao, W., Mugge, L., Vafiadaki, E., Sanoudou, D., Rubinstein, J., Lebeche, D., Hajjar, R., Sadoshima, J., and Kranias, E. G. (2018) HAX-1 regulates SERCA2a oxidation and degradation. *J. Mol. Cell. Cardiol.* **114,** 220–233 CrossRef Medline
31. Vafiadaki, E., Arvanitis, D. A., Pagakis, S. N., Papalouka, V., Sanoudou, D., Kontrogianni-Konstantopoulos, A., and Kranias, E. G. (2009) The anti-apoptotic protein HAX-1 interacts with SERCA2 and regulates its protein levels to promote cell survival. *Mol. Biol. Cell* **20,** 306–318 CrossRef Medline
32. Lam, C. K., Zhao, W., Cai, W., Vafiadaki, E., Florea, S. M., Ren, X., Liu, Y., Robbins, N., Zhang, Z., Zhou, X., Jiang, M., Rubinstein, J., Jones, W. K., and Kranias, E. G. (2013) Novel role of HAX-1 in ischemic injury protection: involvement of heat shock protein 90. *Circ. Res.* **112,** 79–89 CrossRef Medline
33. Ortiz, D. F., Moseley, J., Calderon, G., Swift, A. L., Li, S., and Arias, I. M. (2004) Identificaiton of HAX-1 as a protein that binds bile salt export protein and regulates its abundance in the apical membrane of Mardin-Darby canine kidney cells. *J. Biol. Chem.* **279,** 32761–32770 CrossRef Medline
34. Chen, S.-J., Sanmiguel, J., Lock, M., McMenamin, D., Draper, C., Limberis, M. P., Kassim, S. H., Somanathan, S., Bell, P., Johnston, J. C., Rader, D. J., and Wilson, J. M. (2013) Biodistribution of AAV8 vectors expressing human low density lipoprotein receptor in a mouse model of homozygous familial hypercholesterolemia. *Hum. Gene Ther. Clin. Dev.* **24,** 154–160 CrossRef Medline
35. Khan, A. U. H., Allende-Vega, N., Gitenay, D., Gerbal-Chaloin, S., Gondeau, C., Vo, D.-N., Belkahla, S., Orecchioni, S., Talarico, G., Bertolini, F., Bozic, M., Valdivielso, J. M., Bejjani, F., Jariel, I., Lopez-Mejia, I. C., *et al.* (2017) The PDK1 inhibitor dichloroacetate controls cholesterol homeostasis through the ERK5/MEF2 pathway. *Sci. Rep.* **7,** 10654 CrossRef Medline
36. Denton, R. M. (2009) Regulation of mitochondrial dehydrogenases by calcium ions. *Biochim. Biophys. Acta* **1787,** 1309–1316 CrossRef Medline
37. Arruda, A. P., Pers, B. M., Parlakgül, G., Güney, E., Inouye, K., and Hotamisligil, G. S. (2014) Chronic enrichment of hepatic endoplasmic reticulum-mitochondria contact leads to mitochondrial dysfunction in obesity. *Nat. Med.* **20,** 1427–1435 CrossRef Medline
38. Egnatchik, R. A., Leamy, A. K., Jacobson, D. A., Shiota, M., and Young, J. D. (2014) ER calcium release promotes mitochondrial dysfunction and hepatic cell lipotoxicity in response to palmitate overload. *Mol. Metab.* **3,** 544–553 CrossRef Medline
39. Kruglov, E. A., Gautam, S., Guerra, M. T., and Nathanson, M. H. (2011) Type 2 inositol 1,4,5-trisphosphate receptor modulates bile salt export pump activity in rat hepatocytes. *Hepatology* **54,** 1790–1799 CrossRef Medline
40. Henkel, A. S., Gooijert, K. E. R., Havinga, R., Boverhof, R., Green, R. M., and Verkade, H. J. (2013) Hepatic overexpression of abcb11 in mice promotes the conservation of bile acids within the enterohepatic circulation.

Am. J. Physiol. Gastrointest. Liver Physiol. **304,** G221–G226 CrossRef Medline
41. Figge, A., Lammert, F., Paigen, B., Henkel, A., Matern, S., Korstanje, R., Shneider, B. L., Chen, F., Stoltenberg, E., Spatz, K., Hoda, F., Cohen, D. E., and Green, R. M. (2004) Hepatic overexpression of murine Abcb11 increases hepatobiliary lipid secretion and reduces hepatic steatosis. *J. Biol. Chem.* **279,** 2790–2799 CrossRef Medline
42. Li, T., Matozel, M., Boehme, S., Kong, B., Nilsson, L.-M., Guo, G., Ellis, E., and Chiang, J. Y. L. (2011) Overexpression of cholesterol 7a hydrolase promotes hepatic bile acid synthesis and secretion and maintains cholesterol homeostasis. *Hepatology* **53,** 996–1006 CrossRef Medline
43. Watanabe, M., Houten, S. M., Wang, L., Moschetta, A., Mangelsdorf, D. J., Heyman, R. A., Moore, D. D., and Auwerx, J. (2004) Bile acids lower triglyceride levels via a pathway involving FXR, SHP, and SREBP-1c. *J. Clin. Invest.* **113,** 1408–1418 CrossRef Medline
44. Miller, W. L. (2007) Steroidogenic acute regulatory protein (StAR), a novel mitochondrial cholesterol transporter. *Biochim. Biophys. Acta* **1771,** 663–676 CrossRef Medline
45. Pandak, W. M., Ren, S., Marques, D., Hall, E., Redford, K., Mallonee, D., Bohdan, P., Heuman, D., Gil, G., and Hylemon, P. (2002) Transport of cholesterol into mitochondria is rate-limiting for bile acid synthesis via the alternative pathway in primary rat hepatocytes. *J. Biol. Chem.* **277,** 48158–48164 CrossRef Medline
46. Pineda Torra, I., Claudel, T., Duval, C., Kosykh, V., Fruchart, J.-C., and Staels, B. (2003) Bile acids induce the expression of the human peroxisome proliferator-activated receptor a gene via activation of the farnesoid X receptor. *Mol. Endocrinol.* **17,** 259–272 CrossRef Medline
47. Ahmadian, M., Wang, Y., and Sul, H. S. (2010) Lipolysis in adipocytes. *Int. J. Biochem. Cell Biol.* **42,** 555–559 CrossRef Medline
48. Cárdenas, C., Miller, R. A., Smith, I., Bui, T., Molgó, J., Müller, M., Vais, H., Cheung, K.-H., Yang, J., Parker, I., Thompson, C. B., Birnbaum, M. J., Hallows, K. R., and Foskett, J. K. (2010) Essential regulation of cell bioenergetics by constitutive $InsP_3$ receptor Ca^{2+} transfer to mitochondria. *Cell* **142,** 270–283 CrossRef Medline
49. Feriod, C. N., Nguyen, L., Jurczak, M. J., Kruglov, E. A., Nathanson, M. H., Shulman, G. I., Bennett, A. M., and Ehrlich, B. E. (2014) Inositol 1,4,5-trisphosphate receptor type II ($InsP_3R$-II) is reduced in obese mice, but metabolic homeostasis is preserved in mice lacking $InsP_3R$-II. *Am. J. Physiol. Endocrinol. Metab.* **307,** E1057–E1064 CrossRef Medline
50. Jeoung, N. H., and Harris, R. A. (2008) Pyruvate dehydrogenase kinase-4 deficiency lowers blood glucose and improves glucose tolerance in diet-induced obese mice. *Am. J. Physiol. Endocrinol. Metab.* **295,** E46–E54 CrossRef Medline
51. Go, Y., Jeong, J. Y., Jeoung, N. H., Jeon, J.-H., Park, B.-Y., Kang, H.-J., Ha, C.-M., Choi, Y.-K., Lee, S. J., Ham, H. J., Kim, B.-G., Park, K.-G., Park, S. Y., Lee, C.-H., Choi, C. S., Park, T.-S., Lee, W. N. P., Harris, R. A., and Lee, I.-K. (2016) Inhibition of pyruvate dehydrogenase kinase 2 protects against hepatic steatosis through modulation of tricarboxylic acid cycle anaplerosis and ketogenesis. *Diabetes* **65,** 2876–2887 CrossRef Medline
52. Wu, C.-Y., Tso, S.-C., Chuang, J. L., Gui, W.-J., Lou, M., Sharma, G., Khemtong, C., Qi, X., Wynn, R. M., and Chuang, D. T. (2018) Targeting hepatic pyruvate dehydrogenase kinases restores insulin signaling and mitigates ChREBP-mediated lipogenesis in diet-induced obese mice. *Mol. Metab.* **12,** 12–24 CrossRef Medline
53. Owen, B. M., Mangelsdorf, D. J., and Kliewer, S. A. (2015) Tissue-specific actions of the metabolic hormones FGF15/19 and FGF21. *Trends Endocrinol. Metab.* **26,** 22–29 CrossRef Medline
54. Wang, H. H., Lammert, F., Schmitz, A., and Wang, D. Q. H. (2010) Transgenic overexpression of Abcb11 enhances biliary bile salt outputs, but does not affect cholesterol cholelithogenesis in mice. *Eur. J. Clin. Invest.* **40,** 541–551 CrossRef Medline
55. Chao, J.-R., Parganas, E., Boyd, K., Hong, C. Y., Opferman, J. T., and Ihle, J. N. (2008) Hax1-mediated processing of HtrA2 by Parl allow survival of lymphocytes and neurons. *Nature* **452,** 98–102 CrossRef Medline
56. Hofmann, S. M., Zhou, L., Perez-Tilve, D., Greer, T., Grant, E., Wancata, L., Thomas, A., Pfluger, P. T., Basford, J. E., Gilham, D., Herz, J., Tschöp, M. H., and Hui, D. Y. (2007) Adipocyte LDL receptor-related protein-1 expression modulates postprandial lipid transport and glucose homeostasis in mice. *J. Clin. Invest.* **117,** 3271–3282 CrossRef Medline
57. Hamlin, A. N., Basford, J. E., Jaeschke, A., and Hui, D. Y. (2016) LRP1 protein deficiency exacerbates palmitate-induced steatosis and toxicity in hepatocytes. *J. Biol. Chem.* **291,** 16610–16619 CrossRef Medline
58. Djouadi, F., Bonnefont, J.-P., Munnich, A., and Bastin, J. (2003) Characterization of fatty acid oxidation in human muscle mitochondria and myoblasts. *Mol. Genet. Metab.* **78,** 112–118 CrossRef Medline
59. Meier, P. J., and Boyer, J. L. (1990) Preparation of basolateral (sinusoidal) and canalicular plasma membrane vesicles for the study of hepatic transport processes. *Methods Enzymol.* **192,** 534–545 CrossRef Medline
60. Labonté, E. D., Kirby, R. J., Schildmeyer, N. M., Cannon, A. M., Huggins, K. W., and Hui, D. Y. (2006) Group 1B phospholipase A2-mediated lysophospholipid absorption directly contributes to postprandial hyperglycemia. *Diabetes* **55,** 935–941 CrossRef Medline